THESIS

MAPPING BURN SEVERITY, PINE BEETLE INFESTATION, AND THEIR INTERACTION AT THE HIGH PARK FIRE

Submitted by

Brandon Stone

Graduate Degree Program in Ecology

In partial fulfillment of the requirements

For the Degree of Master of Science

Colorado State University

Fort Collins, Colorado

Summer 2015

Master's Committee:

Advisor: Michael Lefsky

Monique Rocca
Stephen Leisz

ABSTRACT

MAPPING BURN SEVERITY, PINE BEETLE INFESTATION, AND THEIR INTERACTION AT THE HIGH PARK FIRE

North America's western forests are experiencing wildfire and mountain pine beetle (MPB) disturbances that are unprecedented in the historic record, but it remains unclear whether and how MPB infestation influences post-infestation fire behavior. The 2012 High Park Fire burned in an area that's estimated to have begun a MPB outbreak cycle within five years before the wildfire, resulting in a landscape in which disturbance interactions can be studied. A first step in studying these interactions is mapping regions of beetle infestation and post-fire disturbance.

We implemented an approach for mapping beetle infestation and burn severity using as source data three 5 m resolution RapidEye satellite images (two pre-fire, one post-fire). A two-tiered methodology was developed to overcome the spatial limitations of many classification approaches through explicit analyses at both pixel and plot level. Major land cover classes were photo-interpreted at the plot-level and their spectral signature used to classify 5 m images. A new image was generated at 25 m resolution by tabulating the fraction of coincident 5 m pixels in each cover class. The original photo interpretation was then used to train a second classification using as its source image the new 25 m image. Maps were validated using k-fold analysis of the original photo interpretation, field data collected immediately post-fire, and publicly available classifications.

To investigate the influence of pre-fire beetle infestation on burn severity within the High Park Fire, we fit a log-linear model of conditional independence to our thematic maps after

controlling for forest cover class and slope aspect. Our analysis revealed a high co-occurrence of severe burning and beetle infestation within high elevation lodgepole pine stands, but did not find statistically significant evidence that infected stands were more likely to burn severely than similar uninfected stands. Through an inspection of the year-to-year changes in the class fraction signatures of pixels classified as MPB infestation, we were able to observe increases in infection extent and intensity in the year before the fire. The resulting maps will help to increase our understanding of the process that contributed to the High Park Fire, and we believe that the novel classification approach will allow for improved characterization of forest disturbances.

TABLE OF CONTENTS

1. INTRODUCTION

1.1. Overview

Current climate change projections suggest that large intense wildfires will become more frequent and have a greater influence on the western forests in the Rocky Mountains (Garfin et al., 2014). At the same time, climate change appears to be increasing the intensity and extent of bark beetle outbreaks, as increased minimum winter temperatures allow an additional life-cycle each year and facilitate their spread to higher elevations and latitudes (Garfin et al., 2014).

With increased potential for both beetle and wildfire disturbances, it is important that we understand the geographic factors that influence their occurrence and co-occurrence on landscapes. A first step in studying these interactions is mapping regions of beetle infestation and post-fire impacts on vegetation. In this work, we implement an approach for mapping these disturbances for the High Park Fire and investigate the influence of pre-fire beetle infestation on fire severity.

1.2. Mountain Pine Beetle

1.2.1. Background

In the western US, mountain pine beetle (Dendroctonus ponderosae Hopkins) has infected approximately 9.8 million ha of forested areas between 2000 and 2014 (USDA Forest Service, 2015). Mountain pine beetle's historic native range covers most of the pine forests of western North America (Safranyik, 2003). The beetle's primary host is lodgepole pine, but they will attack related coniferous species including ponderosa and whitebark pine (Meddens, Hicke, & Vierling, 2011). Their life cycle consists of larvae developing into a mature adult within the tree's inner bark layer from September through May, and emerging from the host tree and flying

to a new host either within a stand or among stands, depending on the population state (Carroll & Safranyik, 2003). The beetle proceeds to attack and bore into the host tree (August), and if successful in overcoming the tree's natural defenses, they lay eggs to develop over the winter.

As the beetle population expands and collapses it goes through four distinct states: endemic, incipient epidemic, epidemic (outbreak) and post-epidemic (Safranyik, 2003). At low population levels the beetle is considered to be endemic, characterized by attacking weakened and decadent trees with relatively large distances between infested trees. When the population is able to attack a host tree in mass, it enters the incipient epidemic state, as higher beetle counts attack healthier large diameter trees, requiring less travel and create clumps of attacked trees. With sustained population growth, the epidemic state is reached as the infestation becomes widespread and connected across the landscape. Finally, due to either the depletion of host trees or the mass mortality from unfavorable weather conditions, the population peaks and collapses, entering the post-epidemic state and focuses on weakened trees again. The population returns to an endemic state when the population decline stabilizes.

During a mountain pine beetle attack, host trees go through four main stages of decline (Wulder, Dymond, White, Leckie, & Carroll, 2006). In year 1 an "uninfected" host is attacked in August, but displays minimal changes in needle color and is considered to be "green-attack" once killed. During the following winter the larvae develop and girdle the host, causing the needles to fade to a reddish-orange color beginning in May and ending around July of year 2. Over the next 1 to 2 years the red needles drop from the host; when less than 50% of the needles remain, the tree enters the "gray-stage". Finally, in the following years the host tree loses all needles, becoming a standing snag.

The current infestation outbreak in the Colorado Rocky Mountains began as early as 2000, and reached a peak infestation acreage in 2008 (USDA Forest Service, 2015), primarily impacting lodgepole and ponderosa pine stands. The recent expansion has been attributed to regional droughts, forest management practices and increased winter minimum temperatures due to climate change.

Droughts reduce the host trees' ability to fight off the early infestations that target weakened trees within a stand. The US's history of forest management is believed to increase the beetle's infestation attack success rate by creating a forest structure with a higher density of large diameter trees; the primary target for beetle infestation. Historically, minimum winter temperatures have limited the beetle's expansion by killing the developing larvae (Carroll & Safranyik, 2003), but with reduced minimum winter temperatures and increased summer temperatures, the beetle survival rate has increased, and has allowed the beetle population to expand to higher elevations and higher latitudes (Kurz et al., 2008).

The high tree mortality from mountain pine beetle infestations impacts ecosystem services such as carbon storage, biodiversity, water quality, and may influence the forest's response to other disturbances. Forests are a global carbon sink of atmospheric CO_2, as they intake carbon and convert it to fibrous structure tissue. Beetle caused tree mortality causes the stored carbon to be emitted back into the atmosphere through decomposition or wildfire consumption. Kurz et al. (2008) found that beetle impacts converted their study area in the south-central region of British Columbia from a net carbon sink to a net source.

1.2.2. Review of methods

Mountain pine beetle infestations are typically mapped using field sampling, aerial detection surveys or classification of remotely sensed imagery. Given favorable mapping

conditions and crew experience, field sampling would be the most accurate and provide the most detailed information, but it is often limited in spatial extent. Aerial detection surveys can be a useful tool for landscape scale management planning, but doesn't provide the necessary accuracy or detail for stand level analyses (Wulder et al., 2006). To map large landscapes with reasonable precision, recent studies have heavily utilized the classification of remotely sensed imagery in order to map beetle infestation (Wulder et al., 2006; Meddens et al., 2011; Walter & Platt, 2013; Meddens & Hicke, 2014).

Beetle infestation can be mapped using either a single date of imagery or a multi-date change detection approach. Within a single date of imagery, there are several spectral features that can be used to identify the main stages of the beetle infestation, although these spectral features are shared with other types of forest disturbances. Uninfected trees are primarily distinguished by their strong red-edge signature (i.e., low red reflectance and high near-infrared reflectance). Green-attack trees are typically not identifiable within a single image because they exhibit minimal spectral changes in the visible and near-infrared spectrum; only a very subtle change in the near-infrared and shortwave-infrared due to the differences in the moisture content within the needles (Cheng, Rivard, Sánchez-Azofeifa, Feng, & Calvo-Polanco, 2010).

Red-attack trees are the most distinct infection stage, characterized by a decrease in green reflectance and increase in red reflectance, and a reduction in near-infrared reflectance, resulting in a reduced red-edge signature. The gray-attack stage is observed as a transition from the red-attack signature to the ground or understory vegetation signature. Due to the lack of a unique spectral signature, gray-attack trees are typically not identifiable using a single image acquisition.

Utilizing multiple scenes captured across two or more years, we can further identify each infestation stage by following each pixel's temporal trajectory. Uninfected trees generally exhibit a consistent yearly spectral signature prior to the infestation, while red-attack trees are identifiable by a sharp change in their spectral qualities. If the first year of red-attack is found, then the prior year can be assumed to be the initial year of infestation and in the interim the tree was in the green-attack stage. Similarly, gray-attack conditions can be expected to occur during 1 to 2 years following the red-attack year; dependent on regional and species specific variations. An approximation of the gray-attack timing can be identified by using the time-series to find the middle point in the change of red-attack signature (Meddens & Hicke, 2014), or time since first attacked.

The timing of the imagery collection is essential to understanding the measureable stages of infestation and identifying the spectral features with the greatest potential for image analysis. It is typically best to use images taken prior to, or following, the green- to red-attack transition (e.g., a June image would be less useful because it might contain a variable red-attack signature). Images from within the growing season can provide a strong contrast between uninfected and red-attack trees, except when infestation is sparse (e.g., during the endemic population state) where the contribution from uninfected trees may dominate the spectral qualities of the pixel. The inclusion of spring and fall images in a multi-date analysis can be leveraged to help distinguish coniferous from deciduous vegetation and other non-target cover types.

The number of independent spectral bands in the imagery influences the number of infestation stages that can be accurately sampled. The combination of three visible bands and a near-infrared band are most often used to identify uninfected and red-attack within a single image, or up to all four stages if multiple images are used. The addition of a narrow shortwave-

infrared band can help to facilitate the identification of green-attack (Cheng et al., 2010). Hyperspectral imagery has been used to accurately map all four stages of beetle infestation from a single image, but is infrequently used due to its high cost and low availability.

The spatial resolution of the imagery also influences the classification. Imagery with spatial resolution of one meter or less will have multiple pixels within a tree crown that can contain different spectral signatures (e.g., illuminated and shadowed sides; Wulder et al., 2006; Meddens et al., 2011). Alternatively, as the resolution of the imagery exceeds the average tree crown size, the spectral response of the pixels becomes a mixture of cover types and infestation stages (Lefsky & Cohen, 2003). This may limit the ability to identify infestation in the endemic state, and require spectral unmixing or a multi-date approach (Wulder et al., 2006). Spatial resolution is also important for understanding what the final data product represents on the landscape. As pixel size increases, there is greater potential for confusion between the case of a moderate level of beetle infestation throughout the pixel and the case of high beetle infestation within a subset of the pixel.

Given those influences, selecting the correct imagery is a balance between cost, resolution and availability; typically as resolution approaches one meter, the cost increases significantly and the archive availability is limited to populous areas due to the high cost of bandwidth and storage.

1.3. Wildfire

1.3.1. Background

The Rocky Mountains have reportedly experienced an expansion of wildfires over the past decades with trends of increased frequency, extent and intensity (Schoennagel, Veblen, & Romme, 2004). There are three primary factors controlling wildfires: weather, fuels and ignition

source. Within an ecosystem the controlling factors and local species composition help to define a fire regime that outlines how the ecosystem influences and recovers from a wildfire disturbance. Recent anthropogenic changes may have altered the controlling factors of our forests' fire regimes to varying degrees.

Historically there have been three main fire regimes within the Rocky Mountains: low-severity, high-severity, and mixed-severity (Schoennagel et al., 2004). It has been argued that the policy of active suppression of wildfires has resulted in increased fuel density and canopy connectivity (Keane et al., 2002), allowing established wildfires to sustain themselves more than in the past. However Schoennagel et al. (2004) argue that those management decisions have only impacted lower elevation areas that are typically dominated by frequent low-severity fires. They point out that the regions with a history of high-severity fires (e.g., lodepole pine stands) typically experienced the stand replacing events too infrequently for the relatively recent fire suppression efforts to be significant.

For areas prone to low-severity fires, the active suppression of wildfires has significantly increased stand density and canopy connectivity, allowing the fires to enter the canopy and become a high-severity fire (Schoennagel et al., 2004). The frequent nature of the low-severity fires was primarily controlled by fine fuels, and not weather conditions, meaning that a change in forest management has the potential to improve these areas, and that they are not at as a severe of a risk due to climate change. In areas prone to high-severity fires, climatic variation has the largest effect on fire frequency and severity. Recent climatic shifts have the potential to increase the rate of high-severity fires by producing more extreme drought events, reducing fuel moisture and increasing the chance of ignition.

The impact of wildfires on the forest ecosystem varies with burn severity. Impact severity can be broadly separated into impacts on soils and vegetation. Four severity categories are commonly used: unburned, low, moderate and severe.

Low severity burning is typically characterized as a fast moving surface fire consuming minimal understory vegetation. They are considered a natural disturbance regime in dry ponderosa pine forests, occurring at short intervals, limiting the number of saplings and helping to maintain an open canopy structure (Schoennagel et al., 2004).

At low severity levels the dominant canopy vegetation survives with minor charring to its stem and lower branches. Understory vegetation (e.g., shrubs, forbs and tree saplings) experiences the consumption of aboveground biomass with minimal destruction of their root structures, allowing them to rapidly regenerate after the fire. With the conversion of the understory biomass to carbon and basic nutrients during a low severity burn, soils can experience a net benefit of increased nutrient content with a minimal loss of microbes due to the low heat output.

Moderate severity burning is typically due to a surface fire that moves more slowly than a low severity fire and consumes understory vegetation. The needles and braches of canopy vegetation are also scorched during moderate severity burning, and sometimes causes tree mortality. The aboveground portion of understory vegetation is fully consumed by the fire with a fraction of the plants' root structure surviving, primarily large deep rooted shrubs. With a higher percentage of the plant material being consumed by the fire, soils may suffer heat damage to the upper layers, especially where fallen timbers smoldered on the forest floor. The risk of flooding and erosion is increased due to the lack of vegetation and root structures.

Severe burning is the most destructive to the forest and is typically a slow moving canopy fire that fully consumes the forest canopy. Lodepole pine forests have adapted to these infrequent stand replacing fires by utilizing serotinous cones that remain on the tree until heated by a fire enough to remove the thick resin, releasing the seeds and regenerating the entire forest at once.

At the severe level, the aboveground biomass of both the canopy and understory vegetation and the root structure are killed. Vegetation typically regenerates from specially adapted seed sources (e.g., lodgepole pine) or from an outside seed source. Organic matter from the upper soil layers is completely consumed while also killing most of the soil microbes. There is a high potential for increased storm runoff and erosion following the fire.

In extreme cases, the entire soil layer can be sterilized with the surface layer becoming hydrophobic, creating a higher risk for flash flooding and severe erosion. Vegetation regeneration is severely hindered by the loss of soil.

1.3.2. Review of methods

In the United States, standardized burn severity maps are produced by two separate governmental interagency collaborations. The Burned Area Reflectance Classification (BARC) map is produced by the Burned Area Emergency Response (BAER) team, a collaboration between the United States Forest Service (USFS) Remote Sensing Applications Center (RSAC) and the USGS Center for Earth Resources Observation and Science. There is also the Rapid Assessment of Vegetation Condition after Wildfire (RAVG) group, which is supported by the National Forest System Region 5 (covering California) and the USFS RSAC.

The BARC and RAVG maps require pre-fire and post-fire remotely sensed images that have near-infrared (NIR) and mid-infrared (MIR) bands, which generally limits the choice of images to 30 m Landsat Thematic Mapper (TM) imagery. TM band 4 (760-900 nm) is

commonly used as the NIR band while TM band 7 (2,080-2,350 nm) is commonly used as the MIR band.

BARC is meant to map the fire's impact on soils, or soil severity, by using the Differenced Normalized Burn Ratio (dNBR), and is calculated as:

$$NBR = \frac{NIR-MIR}{NIR+MIR} \qquad (1)$$

$$dNBR = NBR_{pre} - NBR_{post} \qquad (2)$$

RAVG is meant to map the severity of the fire's impact on vegetation loss by using the Relative Differenced Normalized Burn Ratio (RdNBR), a modification of dNBR proposed by Miller & Thode (2007).

RdNBR adds a component that relates the estimated NBR to the amount of vegetation available to burn, resulting in a continuous metric that measures relative vegetation loss. It is calculated as:

$$RdNBR = \frac{dNBR}{\sqrt{ABS(NBR_{pre})}} \qquad (3)$$

The BARC and RAVG maps have drawbacks that may limit their availability and application. The requirement of a MIR band generally limits these analyses to the use of Landsat imagery, which limits the spatial resolution to 30 m and, for studies in the years between 2003 and 2014, often requires the use of Landsat 7 images that were affected by the "Scan Line Corrector" problem (USGS, http://landsat.usgs.gov/products_slcoffbackground.php; accessed 6 June 2015). The requirement of a pre-fire image often excludes the possibility of commercial sensors that do not regularly collect imagery; only after a disturbance occurs are commercial sensor tasked to the area. The recently launched DigitalGlobe WorldView-3 satellite, which has high resolution NIR and MIR bands (1.24 m), could serve as an alternative to Landsat but for the immediate future will lack the necessary pre-fire image for most areas.

The use of a pre-fire and post-fire image assumes that the loss of vegetation greenness and gain of soil signature is directly attributable to the wildfire, an assumption that is often not satisfied but is disregarded due to limited imagery availability or the need for images from particular seasons. Disturbances that occur between the collection of the pre-fire image and the fire will be attributed to the fire which will overestimate its area and severity. Similarly, vegetation recovery that occurs after the fire but before the collection of the post-fire image will reduce apparent burn severity.

1.4. Disturbance interactions

1.4.1. Background

The interactions of ecosystem disturbances can be characterized as linked disturbances, compound disturbances or a combination of the two (Schoennagel T., seminar, April 7, 2015; Simard, Romme, Griffin, & Turner, 2011). Linked disturbances relate to the occurrence of an ecosystem disturbance (e.g. beetle infestation) that increases the likelihood, extent or severity of another disturbance (e.g. wildfire). Compound disturbances relate to the co-occurrence of multiple disturbances that influences the ecosystem in a manner that is significantly different then would occur from each individual disturbance (Paine, Tegner, & Johnson, 1998).

Hypothesized causes for linked disturbances between beetle infestation and wildfire include: increased probability of crown fires in beetle infected stands due to increased dead fuels (Simard et al., 2011; Hicke, Johnson, Hayes, & Preisler, 2012), increased burn extent due to beetle infestation (Hart, Schoennagel, Veblen, & Chapman, 2015), increased burn severity in beetle infected stands, and increased future susceptibility of stands to beetle infestation due to the creation of similar aged stands following stand replacing wildfires (Schoennagel T., seminar, April 7, 2015). Hypothesized compound disturbance interactions include: lower tree regeneration

following wildfires in the presence of pre-fire beetle infestation, beetle influences on seed sources and higher impact to forest soils due to increased pre-fire surface fuel loads.

Hicke et al. (2012) found 39 published studies containing evidence about the potential beetle and wildfire disturbance linkages. They point out that the current literature is limited and lacks agreement about the impacts of beetle infestation on fuels and fire. In particular, there is a need for more research on the linkages related to the red-attack stage; most studies focused on the gray stage, post-gray stage or a combination of the red and gray stages.

1.4.2. Review of methods

Research on the interactions of beetle and wildfire disturbances can generally be separated by their method (experimental or case study), and scale (individual tree, hillslope, landscape or continental). Experimental studies focus on understanding specific potential differences in one aspect of interaction (e.g. combustibility of infected vs. uninfected needles) or modeling of interaction scenarios that have not occurred on the landscape or cannot be adequately studied in the field (e.g. due to inability to monitor key processes). Alternatively, case studies focus on using actual disturbance events to quantify the impacts of hypothesized disturbance linkages or to monitor the post-disturbance recovery for hypothesized compound disturbances. While both study approaches are vital for understanding the actual current and potential future impacts, we must always consider that contradictory results from studies using different methods are possible and likely due to the varying real world conditions and importance of different drivers relative to others (e.g. weather might influence fire behavior greater than beetle infestation during drought periods).

The scale of a study is important for understanding the significance of the findings relative to the potential impacts of the interactions. Tree level interactions might alter local burn severity, but have no measureable impact at the landscape or continental scale.

Case studies of beetle and wildfire interactions are often limited to low resolution imagery, aerial detection surveys or field surveys for input layers. The extent and resolution of the input layers influence the scale at which the interactions can be studied. Low resolution imagery and aerial surveys are only appropriate for landscape and continental scale studies; field surveys are appropriate for most scales, but are often prohibitively expensive to implement for heterogeneous ecosystems at a landscape or continental scale.

Recent landscape and continental scale case-studies of beetle and wildfire interactions have begun to utilize input data layers derived from remotely sensed imagery (Hart et al., 2015). As the accessibility to remotely sensed data and the classification methods of disturbance factors are refined, remote sensing has a great potential to help increase our understanding of the interactions.

1.5. Mapping considerations

Analyses that relate image values to field data generally represent the spectral qualities of the field plot with the mean value of the pixels within the plot's spatial extent, and may also incorporate a buffer of pixels adjacent to the plot. These approaches are justifiable if pixels are relatively similar in spectral qualities and that any pixel-to-pixel variability is due to sensor noise or local shadowing effects which will be reduced by averaging. When a buffer is used, it is sometimes justified as a way to minimize the impact of geolocation error in the case of spatial heterogeneity at a spatial scale greater than the field plot.

Classification accuracy statistics for this type of analysis are generally derived using these average pixel values, but final thematic images are very often created at the level of individual pixels, in which case the pixels do not have the accuracy indicated by the plot level accuracy assessment. This approach potentially over-estimates accuracy. An additional potential drawback is that average spectral values are difficult to interpret when the pixels being averaged may either be similar (in which the assumption that an average pixel can represent individual pixels is better approximated) or highly variable (in which case the assumption is violated). Finally, information about the variability of pixels may be lost using this approach.

In this work, we attempt to address these limitations through explicit analyses at both pixel and plot level. As described above, plot level spectral values were generated and used with aerial photo and field data to create and verify a plot-level classification. The resulting classification rules were then applied to individual 5 m pixels. A second image was created at 25 m resolution, where each band represents the proportion of coincident 5 m pixels in each of the original classes. A second classification was developed using the proportion image and the original field data. The advantages of this approach include 1) the creation of a moderate (25 m) resolution image of continuous values representing class proportions that can be analyzed to find yearly trends, 2) the creation of a moderate (25 m) resolution data product with appropriate validation and 3) the ability to use non-square gridding.

1.6. Objectives

The objectives for this study were: develop a robust classification methodology for mapping disturbances to forest ecosystem vegetation; map pre-fire beetle infestation and post-fire vegetation burn severity for the 2012 High Park Fire; validate and compare our classification maps against independent maps; and examine the potential disturbance linkages for the study area.

2. METHODS

2.1. Overview

We created high resolution maps of beetle infestation and burn severity using 15 m plots and 5 m RapidEye imagery using a two stage method. In the first stage, we collected thematic training data for plots through photo interpretation, calculated average spectral values for each plot, and trained a plot-level decision tree classification model ("tier-1" analysis). The tier-1 classification model was then applied to spectral values for individual 5 m image pixels, and the fraction of 5 m pixels associated with each class was calculated for each plot ("class fraction signatures"). A second classification model ("tier-2" analysis) was trained using the same plot-level photo interpretation and these class fraction signatures. The resulting model was applied to each plot and to class fraction signatures calculated at a 25 m resolution. We then analyzed the spatial distribution of MPB infestation, burn severity, and their co-occurrence in the context of the study area's varying biological and physical environment.

These methods utilized data at three different levels of spatial resolution. The 5 m pixel-level matches the native resolution of the imagery and covered the extent of the study area. The plot-level resolution consisted of all 5 m pixels whose center was completely contained within a 15 m radius plot (29 pixels, 725 m^2). Finally, a 25 m spatial resolution was defined as a 5 x 5 grid of 5 m pixels (25 pixels, 625 m^2). The 25 m resolution approximates the training plot area but covers the entire study area with uniform geometry, and was used for the final data products.

At each step of the process, we analyzed model performance statistics and also compared the training data and final data products to independent datasets. For model statistics we primarily focused on class accuracy, model accuracy and the kappa statistic. K-fold cross-

validation was applied to models at both tiers. Comparisons were conducted to independent datasets, including: field data, aerial detection surveys and Landsat derived classification maps produced by other researchers.

To demonstrate the application of the data products and understand the complexities of the High Park Fire, we conducted a coarse analysis that looked at how the MPB infestation and wildfire disturbances interacted. At the 25 m pixel-level, we subset the data into three major forest types and classes based on various aspects of the local physical environment, and then analyzed the spatial distribution of disturbances and their co-occurrence.

2.2. Study site

2.2.1. High Park Fire

The High Park Fire (HPF) location is in the Foothills of the Rocky Mountains just west of Fort Collins, Colorado, bounded approximately by Colorado highway 14 and 44H on the north and south sides, respectively, and country road 63E and the city of Fort Collins on the east and west sides (Figure 2-1a). The fire began on June 9th, 2012 and continued to expand until it was declared 100% contained on July 1st, 2012 after burning an estimated 35,322 hectares (InciWeb, http://inciweb.nwcg.gov/; accessed 27 January 2015).

2.2.2. Geography and forest composition

The burn scar ranges from 1,585 to 3,140 m in elevation, with higher elevations primarily located in the western portion of the area (Figure 2-1b). According to the LANDFIRE Existing Vegetation Type map, coniferous forests covered 75% of the study area, with ponderosa (Pinus ponderosa) covering 37%, lodgepole (Pinus contorta) covering 11%, and a mixed conifer forest class containing both ponderosa and lodgepole covering 28% of the total area (LANDFIRE,

2014). The lower elevation areas were typically dominated by ponderosa forests, while the higher elevations were dominated by lodgepole forests (Figure 2-1c).

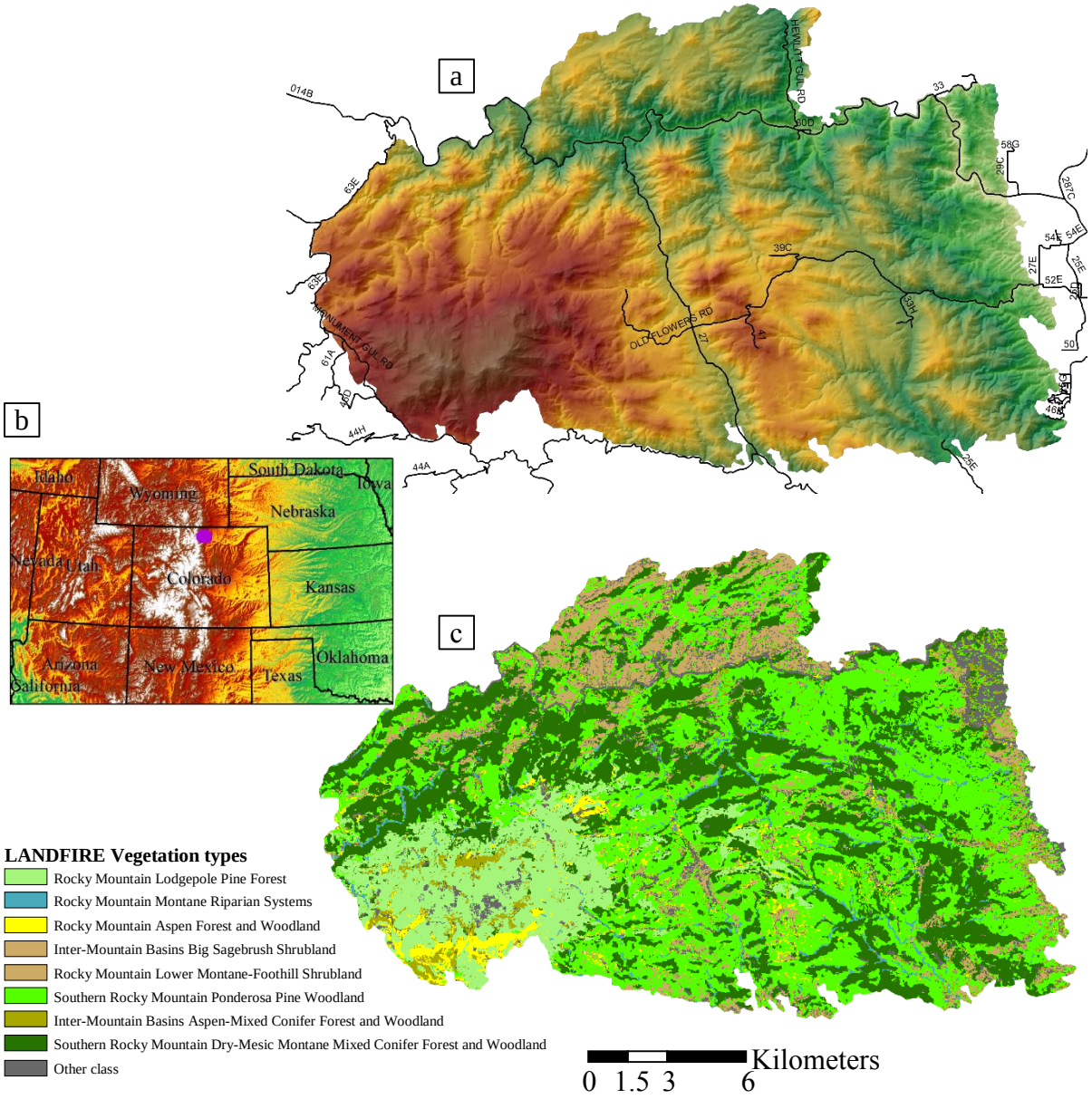

Figure 2-1. (a) Study site location, (b) elevation map and (c) LANDFIRE Existing Vegetation Type map.

2.2.3. Climate and weather

The National Climate Data Center (NCDC) 1981-2010 temperature Climate Normals for the study area were 34.2°F (min.), 45.4°F (avg.) and 56.7°F (max.); the total precipitation

Climate Normal was 21.62 inches (Buckhorn Mountain Station, 1 E, CO US; 40.6158°N, 105.2969°W). The three closest Remote Automatic Weather Stations (Table 2-1; RAWS, http://www.raws.dri.edu/; accessed 1 December 2014) indicated that the months leading up to the 2012 fire were drier, warmer and less humid than average (Figure 2-2).

Table 2-1. Remote Automatic Weather Stations neighboring the study site.

RAWS station	Station ID	Latitude	Longitude	Elevation (ft.)	Distance from HPF (km)	Direction from HPF to station
Red Feather, CO	RFRC2	40° 47' 53"	105° 34' 20"	8200	15	NW
Redstone, CO	ESPC2	40° 34' 15"	105° 13' 35"	6082	1	SE
Estes Park, CO	RSOC2	40° 22' 00"	105° 33' 00"	7820	25	SW

In this area, precipitation generally peaks in May and drops to its lowest in December and January (Figure 2-2b). NCDC precipitation data reveals a May precipitation Climate Normal of 3.26 inches and a Jan through May average total of 9.23 in. May 2012 had a total precipitation of 1.19 inches (37% of normal) and a Jan through May total of 4.25 inches (46% of normal) (Western Regional Climate Center, http://www.wrcc.dri.edu/; accessed 1 December 2014).

2.3. Imagery and data layers

2.3.1. Imagery

Background

Multispectral imagery from the RapidEye constellation was selected for this project because it is a high resolution product with a short time between revisits (5.5 days), a global archive of regularly collected scenes starting in 2009, and higher spectral resolution than other sources of imagery with similar spatial resolution (http://blackbridge.com/rapideye/). There are five spectral bands: Blue (440-510 nm), Green (520-590 nm), Red (630-685 nm), Red-edge (690-730 nm), and Near-infrared (NIR; 760-850 nm). The imagery is collected at a 6.5 x 6.5 m

ground sampling distance at nadir, and delivered orthorectified at a 5 x 5 m resolution. The imagery used in this project was delivered as a level 3A orthoregistered product; with radiometric, sensor, and geometric corrections applied by the vendor.

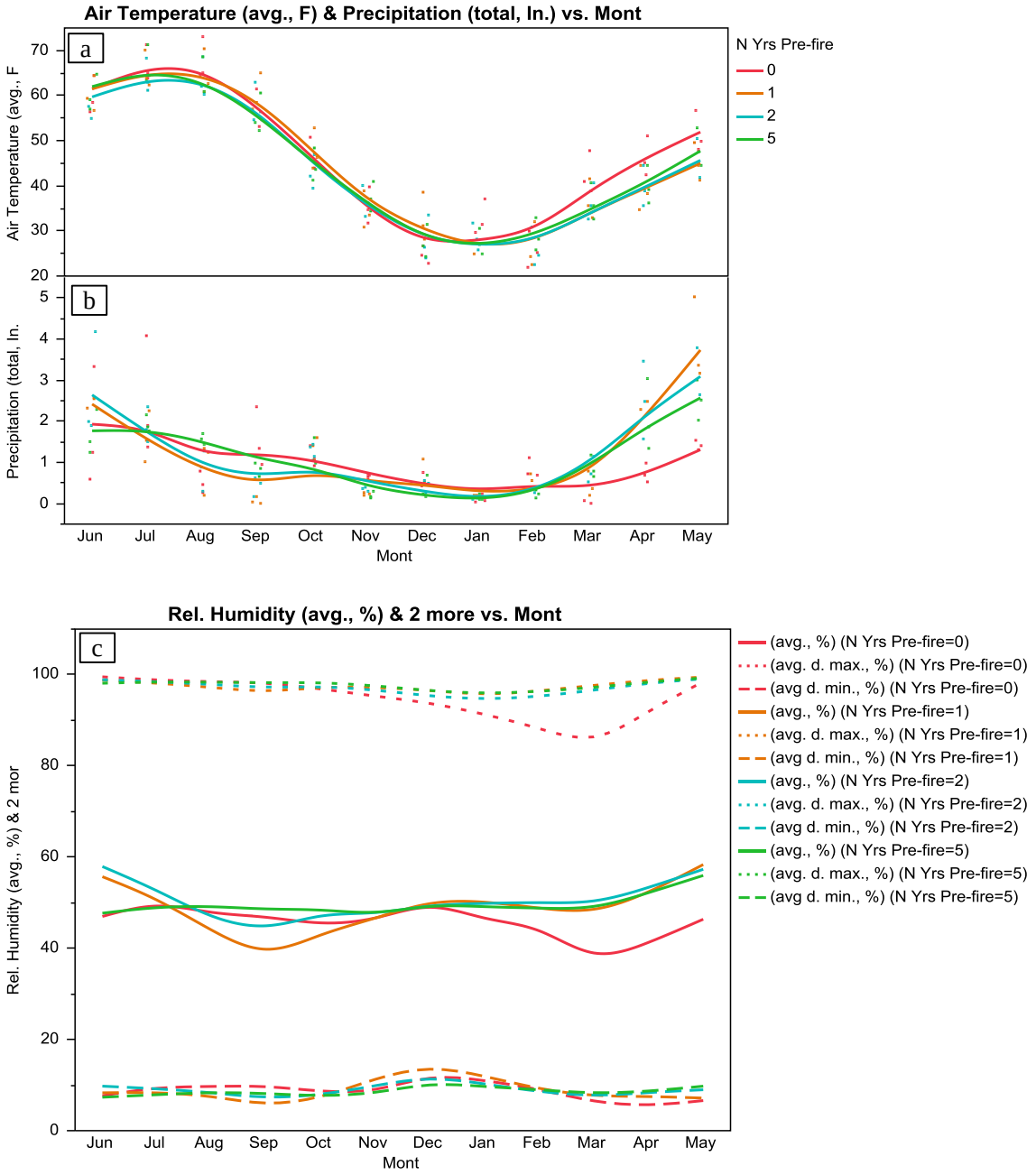

Figure 2-2. June through May weather averages for the periods: 2012, 2011, 2010-2011 and 2007-2011. (a) Mean daily air temperature, (b) total precipitation and (c) mean daily average, minimum and maximum relative humidity.

Preprocessing

Three dates of imagery were selected based on data coverage, availability across years (for MPB) and proximity to the start and end of the HPF (for burn severity): May 8, 2011, May 14, 2012 and July 20, 2012. Preprocessing of the imagery consisted of checking co-registration accuracy and calculating radiance for each band. Co-registration accuracy was tested by iteratively shifting a test image by up to 15 pixels in x and y dimensions and then calculating the correlation of a random subset of pixels from the shifted test image to a reference image. All combination of RapidEye images had the highest correlation value when the shift offset was zero, confirming that the delivered images' geolocation is consistent.

The images were delivered as Digital Number (DN) products and converted to radiance by multiplying the DN by the supplied radiometric scale factor of 0.01. For this analysis the training and application of classification models was restricted to a single image date meaning that, under the assumption of a horizontally homogeneous atmosphere, an atmospheric correction of at-sensor radiance to surface reflectance was not necessary (Song, Woodcock, Seto, Lenney, & Macomber, 2001). To help facilitate the comparison of images and image statistics during our methods development, a histogram based simplified dark-object subtraction model was applied to each image independently as a first order correction for haze (Chavez, 1988). For each image band we used a histogram threshold to select a haze value that was then subtracted from the band; pixels less than the haze value were recorded as no data.

Data masks were created for the three RapidEye images to remove areas of missing or low quality data (e.g., clouds, cloud shadows, and snow). On the May 2011 image, approximately 5% of the HPF burn scar fell outside of the western edge of the image swath, and there was also a localized area of high elevation that had snow cover. The July 2012 image

required that 5% of the burn scar masked out due to cloud cover. The May 2012 image did not require any masking.

2.3.2. Descriptive data layers

Digital terrain model

Topographic information layers were created from a USGS National Elevation Dataset 9 m digital elevation model (DEM; National Elevation Dataset, http://ned.usgs.gov/; accessed 5 May 2014). Elevation was categorized into Lower (1,585 - 2,125 m), Middle (2,125 - 2,325 m), and Upper (2,325 - 3,140 m) classes. The DEM was also used to calculate aspect as degrees from north. Thresholds were selected to create three aspect classes: North (< 60° or > 300°), East-West (60 - 119° or 240 - 299°), and South (120 - 240°). Topographic information layers were then resampled to a 25 m resolution, matching the resolution of the final data products.

Forest composition

Forest composition was obtained from the LANDFIRE Existing Vegetation Type coverage, a 30 m species composition layer based on field data, Landsat imagery, elevation, and biophysical gradient data (Figure 2-1c; LANDFIRE, 2014). The LANDFIRE layer was used for vegetation type comparisons, focusing on the three following conifer forest classes: Southern Rocky Mountain Ponderosa Pine Woodland, Southern Rocky Mountain Dry-Mesic Montane Mixed Conifer Forest, and Woodland and Rocky Mountain Lodgepole Pine Forest (LANDFIRE, 2014).

Two additional vegetation cover classes, aspen and shrubland, were also utilized for some comparisons; the aspen class was comprised of the Rocky Mountain Aspen Forest and Woodland and the Inter-Mountain Basins Aspen-Mixed Conifer Forest and Woodland LANDFIRE classes, while the shrubland class was comprised of the Inter-Mountain Basins Big Sagebrush Shrubland

and the Rocky Mountain Lower Montane-Foothill Shrubland classes. For the purpose of this analysis, the aspen vegetation types were combined into one class, and the shrubland classes were also combined into one class, reducing the total LANDFIRE classes to five.

2.3.3. Field data

Field data was collected in September and October 2012, between two to three months after the fire was extinguished. Field crews sampled 94 20 m x 20 m plots, recording forest biophysical properties including the stage or presence of pre-fire MPB (stage for unburned stems and presence for burned stems), post-fire burned status and diameter at breast height (unpublished data). The field plot locations were recorded with a Trimble Juno 3B. Post-processing of the GPS data indicated a mean horizontal GPS accuracy of 3.1 m with a standard deviation of 2.1 m and a median accuracy of 2.8 m.

2.3.4. Ancillary data layers

Aerial detection survey

The USDA Forest Service conducts aerial detection surveys to map insect, disease and other forest disturbances at regional to national scales (USDA Forest Service, 1950). Meddens and Hicke (2014) outlines three major limitations of the surveys: tree status within the digitized polygons is unknown, making it difficult to assess changes in stand level mortality due to shifting outbreak intensities; interpreter bias; and the lack of yearly data collection for some regions. Our study utilized the survey data to help understand the timeframe of the latest MPB outbreak and the spatial progression during the outbreak.

USDA aerial detection survey maps of MPB infestation for the HPF region indicate a history of outbreak cycles with the most recent outbreak reaching peak acreage around 2009 for lodgepole stands and 2010 for ponderosa stands (Figure 2-3; USDA Forest Service, 1950).

Burned Area Reflectance Classification

A Burned Area Reflectance Classification (BARC) map was used as a comparison for our own burn severity maps. BARC data was created and provided by the Forest Service Burned Area Emergency Response (BEAR) team (R. McKinley, personal communication, December 12, 2012) An initial version of the BARC map was created prior to 100% containment and relied on hand digitization of the western portion of the fire; this project focused on the second version, dated July 23rd, 2012, which was created using a post-fire image, did not use hand digitized areas and had updated class thresholds.

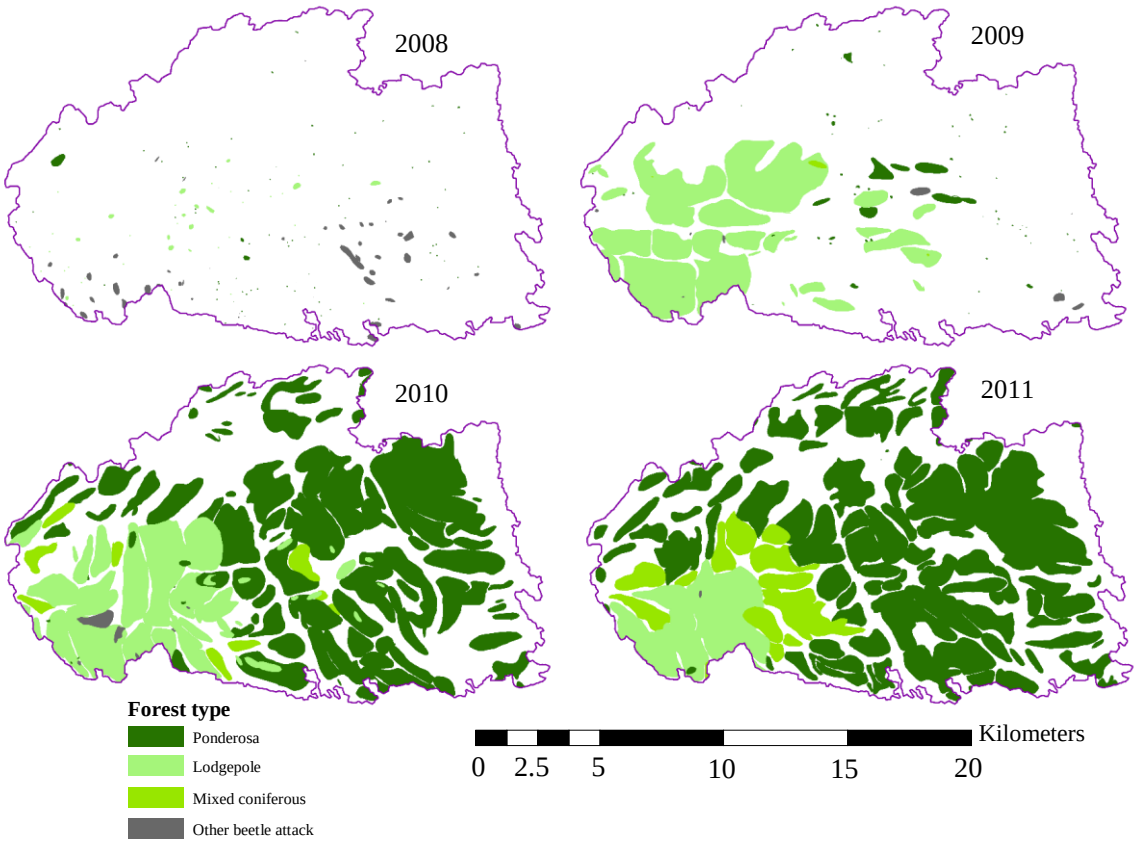

Figure 2-3. Yearly maps of MPB infected stands, colored by forest type, from 2008-2011. (Source: USDA Forest Service aerial detection survey.)

The BARC map leverages the dNBR (Equation 2) metric to classify the burn scar into one of four classes: high, moderate, low and unburned (USGS EROS, 2012). Two Landsat

images were used by the BEAR team to create the HPF BARC map: a pre-fire Landsat 5 scene (June 8th, 2011; path/row 34/32) and a post-fire Landsat 7 scene (July 20th, 2012; path/row 34/32). A 30 m resolution NBR (Equation 1) image was created from each Landsat image and then differenced to create a single dNBR image. The dNBR image was then rescaled from 0 to 255 to create their continuous "BARC256" data product, and lastly classified into the final BARC data product using thresholds chosen by an analyst at USGS EROS.

To allow for a comparison with our burn severity map, the Landsat 7 missing scan lines were marked as no data in all of the BARC data products (Figure 2-4a).

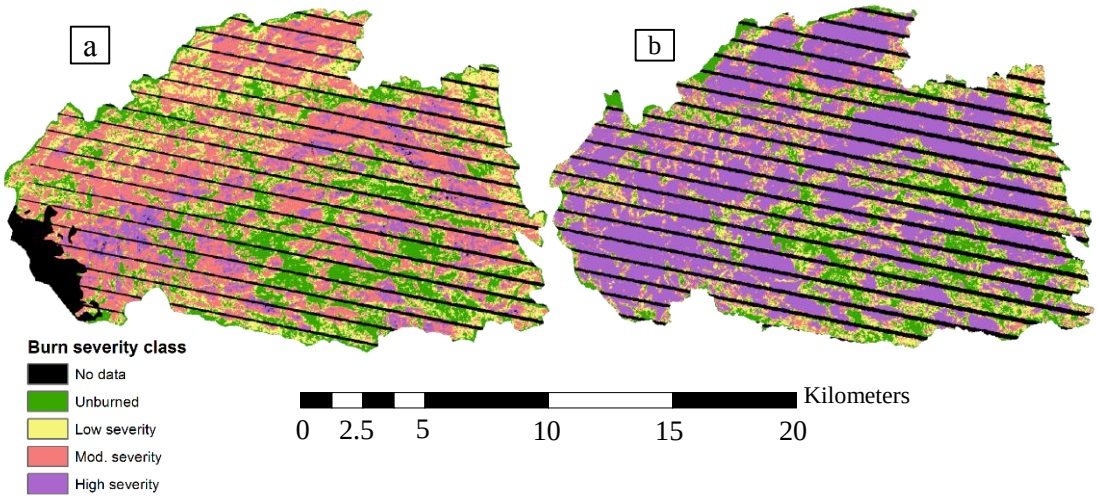

Figure 2-4. Independent burn severity maps of the HPF. (a.) BARC – Four classes. (b.) RAVG – Four classes resampled from classified percent canopy cover mortality.

Rapid Assessment of Vegetation Condition after Wildfire

A Rapid Assessment of Vegetation Condition after Wildfire (RAVG) burn severity map was also used as a comparison for the study and was created by the USDA FS – Remote Sensing Applications Center (RSAC; USDA Forest Service, 2013).

RAVG data products are based on the RdNBR metric, first proposed by Miller and Thode (2007; Equation 3). For the HPF RAVG map, the RSAC team utilized two Landsat images: pre-

fire Landsat 5 scene (August 21st, 2009) and post-fire Landsat 7 scene (August 5th, 2012). NBR images were created from the 30 m Landsat scenes and then used to create a single RdNBR image. From there they created continuous and categorical data products that map change in basal area, change in canopy cover and the severity in Continuous Burn Index units. The layers were calibrated using data from previous fire studies.

We compared the RAVG percent canopy cover mortality product to our own photo interpretation of burn severity (see 2.4.3. Burn severity). To align with our four class burn severity map, we resampled the RAVG layer to the following four classes: unburned (0%), low (0-25%), moderate (25-50% & 50-75%) and severe (>=75%; Figure 2-4b). We then marked the Landsat 7 missing scan lines as no data and excluded them from the comparisons.

2.4. Photo interpretation

2.4.1. General methods

Photo interpretation of the two pre-fire RapidEye images (May 8, 2011; May 14, 2012) focused on assessing mountain pine beetle (MPB) infestation, while the post-fire RapidEye image (July 20, 2012) was used to assess vegetation burn severity. The locations of 456 15 m radius circular plots were selected by using 97 random plot locations from the field sampling and an additional 359 plots selected using a stratified random selection within a rectangular area fit to the fire boundaries (north-west [455500, 4509100], south-east [484800, 4490500]; WGS84, UTM 13N). The stratification was implemented using an early revision of the tier-1 classification model.

Any plots that intersected or were within 100 m of a non-vegetative land cover class (e.g. roads, trails, streams, lakes, urban structures or agriculture lands) were removed from the analysis. In addition, plots that intersected aspen (Populus tremuloides) stands were also

removed from the MPB infestation analysis to prevent MPB commission errors influenced by the seasonal and elevation differences in the timing of deciduous leaf budding. For each image analysis we excluded all plots that contained any missing data pixels (i.e. the May 2011 image was not a complete scene, missing data in the extreme western portion of the study area).

2.4.2. MPB infestation

To assess MPB infestation, the percent of green vegetation cover and the percent of red attack MPB cover was photo interpreted for all plots. The identification of red attack trees followed methods used in similar studies (Wulder et al., 2006; Wulder, Ortlepp, White, Coops, & Coggins, 2009; Meddens et al., 2011), and assumed that in this region and during this period of time, pine mortality was primarily attributable to MPB (J. Negron, USDA Forest Service, personal communication, February 20, 2014). To reduce misclassification errors, additional RapidEye imagery from September 2009 and October 2010 and a one meter 2011 National Agricultural Inventory Program (NAIP, 2006) image were used to identify whether a plot should be excluded from the analysis on the basis of land cover, vegetation health history, or winter vegetation condition (e.g. leaf-off aspen).

Green vegetation cover was defined as the percent of a plot's pixels with a spectral signature clearly indicative of vegetation (e.g. green in true color and red in false-color IR), and was recorded at one of the following levels: 0%, 1-24%, 25-49% and >50%. Red attack cover was defined as the percent of a plot's pixels with a clear signal of vegetation mortality (decrease in green reflectance, increase in red reflectance and a reduction in near-infrared reflectance) and the presence of healthy vegetation in an earlier image. MPB mortality was recorded at one of the following levels: 0%, 1-24%, 25-49%, 50-74% and greater than 75%.

After the photo interpretation was completed, the MPB infestation classes were simplified into one of four classes: bare ground, sparse green vegetation, dense green vegetation, and MPB attack vegetation; examples of which are shown in Figure 2-5. The thresholds used to create the four MPB infestation classes are included in Table 2-2.

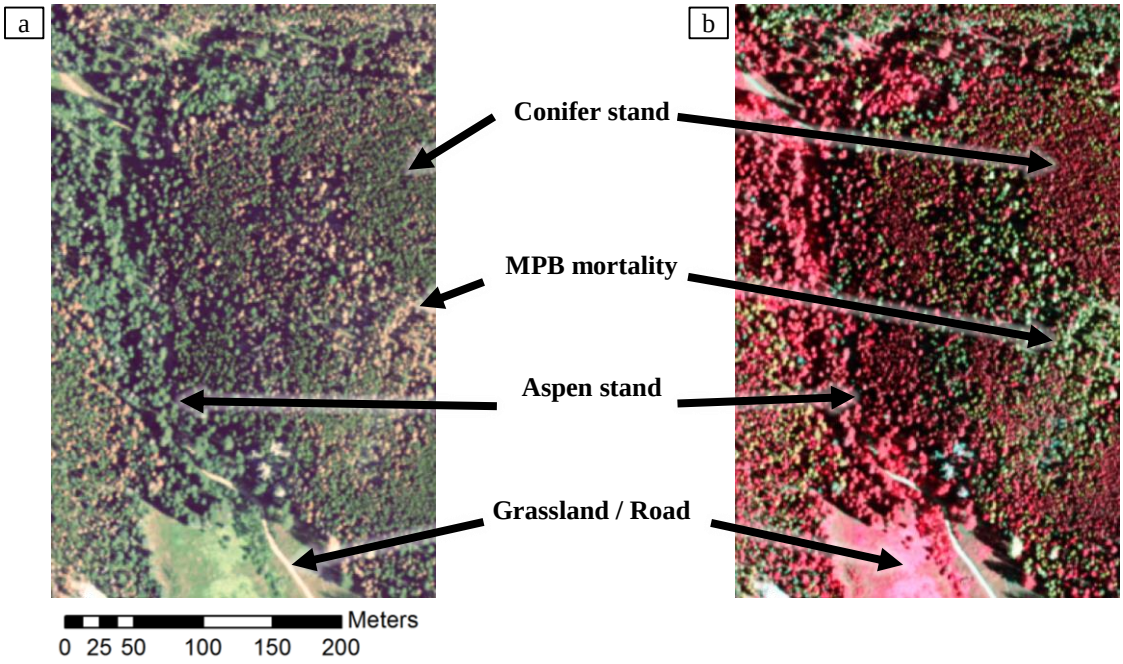

Figure 2-5. Example of MPB infestation in the study area using a 2011 1 m NAIP image displayed as (a) true color and (b) false-color infrared.

Table 2-2. Photo interpretation cover ranges for the four simplified MPB infestation classes.

Cover class	Green vegetation cover	MPB mortality cover
Bare Ground	0%	0%
Sparse Vegetation	1% - 50%	0% - 24%
Dense Vegetation	51% - 100%	0% - 24%
MPB attack	1% - 100%	25% - 100%

The MPB attack class consisted of plots that had vegetation cover greater than 0% and MPB cover greater than 25%. Testing was done using an additional class that would split MPB

attack into a high (>50%) and low (25-50%) cover class, to represent MPB attack intensity, but due to the limited area and intensity of MPB attack in 2011, only a single class could be used. In addition, we tested the use of an emerging MPB attack class that used the 1-24% MPB cover PI category, but the classification models displayed a high confusion rate between emerging MPB attack and sparse vegetation.

2.4.3. Burn severity

The vegetation burn severity map was trained using photo interpreted classes from the July 20th, 2012 RapidEye imagery dataset. Vegetation burn severity was classified as unburned, low, moderate or severe, following the classes first proposed by Ryan and Noste (1985) and subsequently refined by Keeley (2009).

The unburned class represented an area that did not experience any wildfire driven changes. Low severity areas had understory vegetation consumed by the fire, but left the majority of the upper canopy unscorched. Moderate severity areas were scorched, killing the needles, but did not fully consume the canopy. Severe burn areas had complete understory and canopy loss from the wildfire. Each plot was classified into one of the four classes based on the dominant severity class of the entire plot (Figure 2-6).

2.4.4. Validation against field data

We have compared the photo interpretation and mountain pine beetle infestation data to the 97 co-located ancillary field plots.

MPB infestation

Within the ancillary field data we found that a plot's percent of stems classified as pre-fire dead was the most suitable proxy for our area based MPB attack class. The field data

contained a MPB attack status field, but inspection of the data revealed potential issues with post-fire identification of MPB attacked trees, primarily in areas that were severely burned.

Plots were classified into one of two possible classes: healthy (less than 20% pre-fire mortality) or high mortality (greater than or equal to 20% pre-fire mortality). The 20% threshold was determined by the decision tree algorithm and separates the two levels of MPB that could be most accurately determined. A confusion matrix (Congalton, 1991) was produced to compare the field data classes against our MPB attack PI class and a combined class of the remaining three classes (bare, sparse vegetation and dense vegetation).

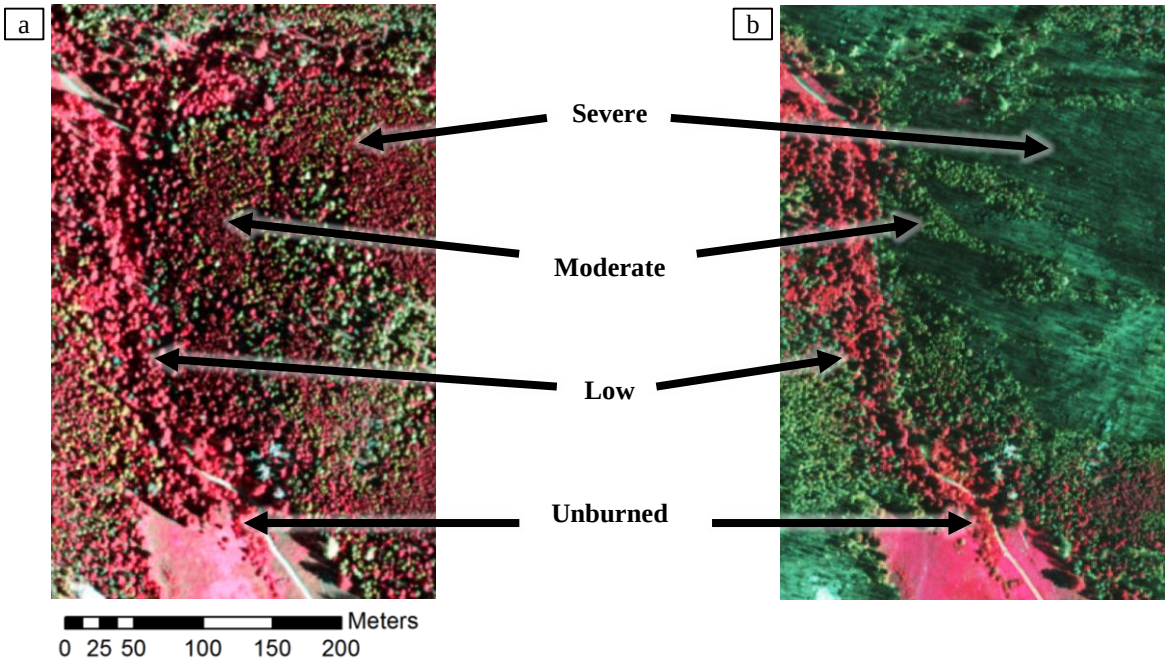

Figure 2-6. Example of burn severity levels (a) before and (b) after the HPF, using a 2011 1 m NAIP image displayed as false-color infrared.

Burn severity

Stems within the ancillary field plots were recorded as one of the following: unburned-alive, burned-alive, burned-dead or prefire-dead. For the burn severity PI validation we classified the field plots into one of four classes by first calculating the percent of stems within a plot that

were either unburned-alive, burned-alive or burned-dead; excluding stems that were recorded as prefire-dead as they could have been burned or unburned. Next, a decision tree with three splits was used to find classification thresholds that aligned with our burn severity results. We found that unburned plots had 100% unburned-alive stems, low severity plots had between 20% and 43% burned-alive stems, moderate severity plots had greater than or equal to 43% burned-alive stems, and severe plots had greater than or equal to 80% burned-dead stems. A confusion matrix was produced to compare the four field data classes against our four burn severity PI classes.

2.5. Classification

2.5.1. C5 classification model background

To classify imagery for the MPB and burn severity analyses, we used the GNU GPL version of the C5.0 decision tree classification model (RuleQuest, http://www.rulequest.com/; Quinlan, 1993). The C5.0 software is a commercial implementation of Ross Quinlan's (1993) original C4.5 algorithm that includes new features and improvements to the size and speed of the decision trees classification models. The C5.0 software, along with similar decision tree implementations, have previously been used to successfully classify remotely sensed imagery (Fry, Coan, Homer, Meyer, and Wickham, 2009; Bricklemyer, Lawrence, Miller, & Battogtokh, 2007). We used C5.0 for this study because of the training and classification performance, the free public availability of the single threaded version, and the ability to handle input variables with different statistical distributions. A maximum likelihood classifier was not used due to its assumption of normal distribution of class signatures (e.g. positive skew of RGI; Huang, Davis, & Townshend, 2002). One benefit of using a decision tree classification model compared to other methods is the output of a human-readable classification model in which we could learn how different input variables were being utilized by the classification model.

2.5.2. Tier-1 classification

Spectral indices

For the tier-1 models we calculated nine RapidEye spectral indices at the 5 m pixel-level and at the plot level. In addition to the five RapidEye band values (Blue, Green, Red, Red-edge and NIR), we used the following spectral indices: Normalized Difference Vegetation index (NDVI), Red Green index (RGI), Normalized Difference Red Edge index (NDRE), and a modification of the NDRE labeled as Normalized Difference Red and Red Edge index (NDRRE). NDVI was calculated as (Tucker, 1979):

$$NDVI = \frac{NIR-Red}{NIR+Red} \qquad (4)$$

where NIR is RapidEye band 5 and Red is RapidEye band 3 reflectance. NDVI was selected because it is a widely used index for assessing vegetation health and greenness at varying levels of landscape illumination (Meddens et al., 2011; Walter & Platt, 2013; Krofcheck et al., 2013; Keeley, 2009). RGI was calculated as (Coops, Johnson, Wulder, & White, 2006):

$$RGI = \frac{Red}{Green} \quad (5)$$

where Green is RapidEye band 2 reflectance. RGI is another measure of vegetation greenness (Coops et al., 2006; Meddens et al., 2011). NDRE (Gitelson & Merzlyak, 1996) and NDRRE were calculated as:

$$NDRE = \frac{NIR-Red\ Edge}{NIR+Red\ Edge} \qquad (6)$$

$$NDRRE = \frac{Red-Red\ Edge}{Red+Red\ Edge} \qquad (7)$$

where Red Edge is RapidEye band 4. NDRE has been used to capture vegetation canopy structure and chlorophyll concentration (Krofcheck et al., 2013).

Classification model

The same general methods were applied to both the burn severity and beetle infestation classifications. For each of the three image dates, tier-1 classification models were trained using the plot-level photo interpretation classes and the plot-level spectral indices. For each model, the individual class accuracies, overall accuracy and kappa statistics were recorded (see 2.5.5. Validation). The attribute usage metric represents each spectral statistic's percent utilization in the decision tree (e.g., if 25% of the plots were MPB infected and only those plots utilized RGI for their classification, the RGI attribute usage would be 25%) and was recorded to understand the importance of the different metrics. Next, the classification model was used to classify the entire study area using the 5 m pixel-level spectral indices. The result was three 5 m categorical classification maps which were only used as an intermediate data product.

2.5.3. Tier-2 classification

Class fraction signatures

To generalize the 5 m pixel-level class map to the plot-level and 25 m pixel-level, we calculated "class fraction signatures"- the proportion of all 5 m pixels associated with either a plot or 25 m pixel that was classified as each of the tier-1 classes, ranging from 0 to 1. For this study, each set of class fraction signatures contained four variables, based either on the MPB infestation (bare ground, sparse vegetation, dense vegetation, MPB attack) or burn severity (unburned, low, moderate, severe) classes.

Class fraction signatures were calculated at two different resolutions. It was calculated at the plot-level, utilizing the 5 m pixels whose center overlapped the plot area. The average class fraction signatures for each photo-interpreted training class were recorded for inspection. It was

also calculated using a 25 m pixel size, where each pixel utilizes 25 5 m pixels. The two resolutions are approximately equivalent in total area, 725 m^2 and 625 m^2, respectively.

Classification model

To train the tier-2 classification model, we used the original thematic classes along with the set of plot-level class fraction signatures. As with the tier-1 classification model, we recorded the individual class accuracies, overall accuracy and kappa statistic for each tier-2 classification model. Each class fraction signature's percent utilization in the decision tree was recorded to understand the importance of the different cover types. A 25 m pixel-level map of the study area was produced for each image date by classifying the 25 m pixel-level class fraction signatures with the tier-2 classification models.

2.5.4. Data products

MPB infestation over two years

The final MPB infestation class map was created by taking the May 2011 and May 2012 25 m pixel-level class maps and combining their respective classes. This combined map replaced the single MPB attack class with two new classes, late stage MPB (MPB attack observed in both years) and early stage MPB (MPB attack observed in May 2012 only), expanding the total number of classes to five (Table 2-3).

The literature and expert local opinion indicate that healthy green trees are attacked by MPB in the late summer or early fall, remain green through the winter, and begin to have needles fade by the following June (Wulder et al., 2006; J. Negron, USDA Forest Service, personal communication, February 20, 2014). We used this information to interpret the different class map dates. The early stage MPB classification represents areas that had green trees that were attacked by MPB in 2010, observed in the green attack stage in May 2011, and then observed in

the red attack stage in May 2012, prior to the fire. The late stage MPB attack classification represents areas that had green trees that were attacked by MPB in 2009 or earlier, observed in the red attack stage in May 2011 and then again in May 2012. An example of early vs. late stage red attack is shown in Figure 2-7.

Table 2-3. Two year combined vegetation and MPB cover class definitions.

Two year MPB infestation classes	Class in May 2011	Class in May 2012	Plot counts
Bare Ground	Bare Ground	Bare Ground	52
Sparse Vegetation	Dense Veg., Sparse Veg.	Sparse Veg.	104
Dense Vegetation	Dense Veg., Sparse Veg.	Dense Veg.,	97
Early stage MPB	Dense Veg., Sparse Veg.	Red Attack	62
Late stage MPB	Red Attack	Red Attack	38

It should also be noted that other combinations of the classes in each year are possible and would expand the total number of MPB infestation classes beyond five. Logical class transitions (e.g. sparse vegetation to dense vegetation) were coded as their class from latest image (i.e. May 2012). Improbable class transitions (e.g. MPB attack to dense vegetation) were combined into an "inconsistent" cover class. That class is hypothesized to include errors that arise from deciduous tree differences (e.g. leaf off in 2011 and leaf on in 2012).

Areas where there was only imagery available for a single date (e.g. no coverage, snow, clouds, etc.) were assigned a class from the other date, if available. This can be important to note for the early vs. late stage MPB classes as their distinction becomes unknown; if there was no data in 2011 and MPB attack in 2012, the area could be either early or late stage; for the purpose of our initial analysis, we assumed those areas were early stage MPB.

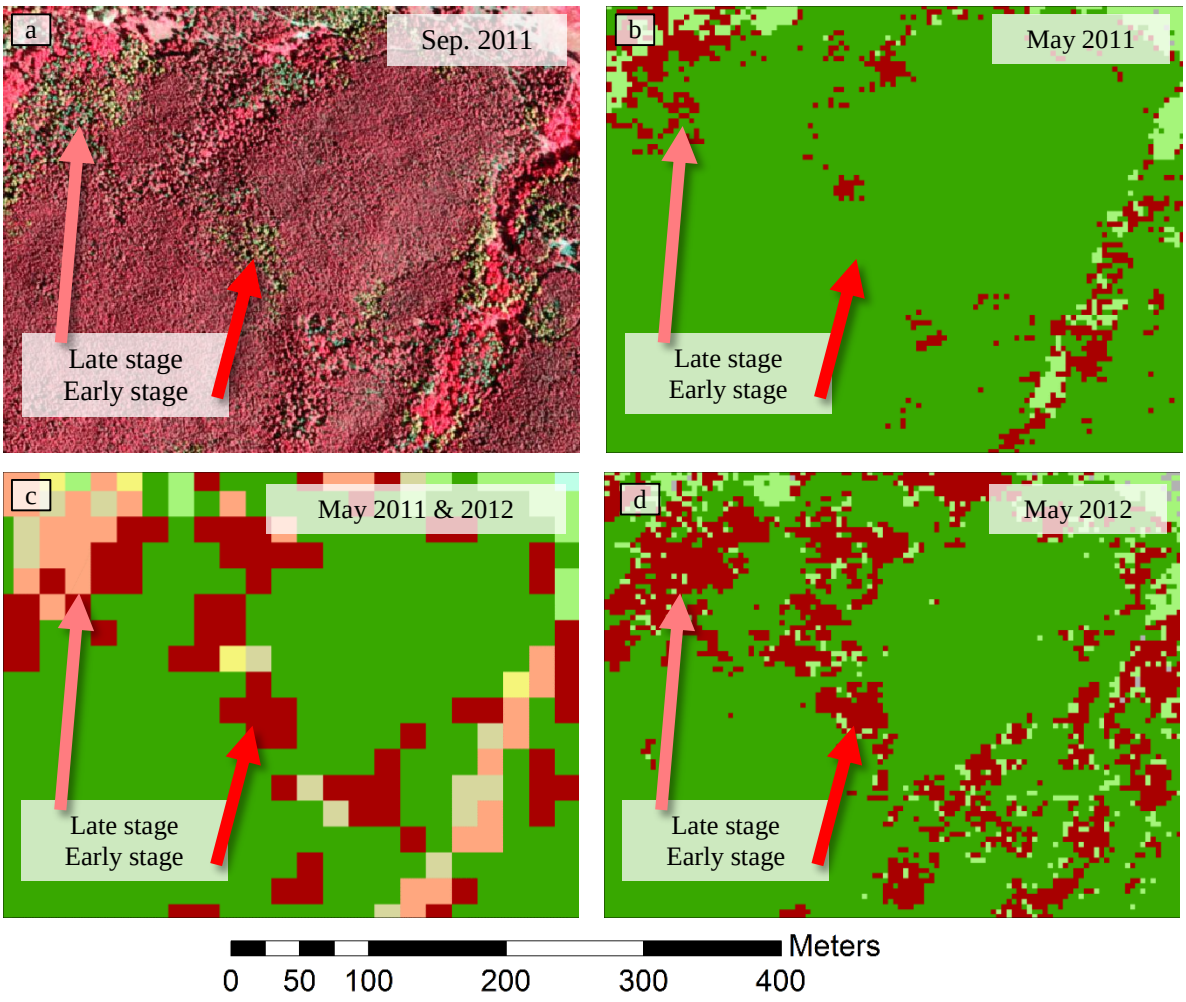

Figure 2-7. Example of a MPB attacked landscape. The image is a one meter NAIP image, displayed as false-color infrared, and was captured in the late summer of 2011. The example plots represent: (a) sparse vegetation, (b) dense vegetation, (c) early stage MPB and (d) late state MPB.

Burn severity

The final burn severity map was created by using the tier-2 25 m pixel-level class map and masking out the areas outside of the fire perimeter. The fire perimeter was created by applying morphological operators to the 25 m class map and outlining the connected regions. A few small hand edits were applied where clouds obstructed the fire perimeter and where the May 2012 Hewlett Gulch fire perimeter intersected with the HPF (USGS EROS, 2012). Areas of no data or missing coverage were also masked out.

2.5.5. Validation

Confusion matrix statistics

A confusion matrix (Congalton, 1991) and set of classification statistics were created for tier-1 and tier-2 classification models for both beetle infestation and burn severity classifications. The statistics included with the confusion matrices are: producers and user accuracy, overall accuracy, and a kappa statistic. The kappa statistic was calculated as (Cohen, 1960):

$$Kappa = \frac{p(a)-p(e)}{1-p(e)} \quad (8)$$

where p(a) represents the overall accuracy and p(e) represents the probability of chance agreement. Meddens et al. (2011) demonstrated how the kappa statistic can be used in conjunction with the Landis and Koch (1977) proposed ordinal kappa scale of agreement "poor" (less than 0.4), "moderate" (0.4 to 0.8) and "strong" (greater than 0.8), to outline the performance of a classification model.

Cross-validation

In addition, a separate set of confusion matrix statistics were calculated using k-fold cross-validation. This analysis was used to determine the classification model's sensitivity to the selection of training data and reveal possible over fitting of the data. The k-fold statistics were created by first randomly partitioning the entire training data set into five subsamples, maintaining equal class proportions. Iteratively, four subsamples were used to train the classification model and classify the remaining subsample, repeated so that every subsample is used to validate the model once. The entire process was repeated ten times to calculate an average and variance for the accuracy statistics. The change found in the k-fold statistics was included in the confusion matrices as the absolute difference in values.

2.6. Map analysis

2.6.1. Mosaic plots

Mosaic plots are a visualization tool for displaying two-way or multi-way frequency tables of categorical data (Hartigan & Kleiner, 1981; Friendly, 1994). For each cell in the table, a rectangle is created whose area is proportional to the observed frequency of the cell. If all frequencies were equal and independent, then all rectangles would be of equal size. A hierarchical ordering of the categorical variables is typically applied to restrict the placement of the rectangles so that the relative proportional frequency of each variable can be deciphered as a user traverses the hierarchy.

Log-linear models may be applied to mosaic plots to test for independence between variables (Friendly, 1999). The most basic model is mutual independence, which keeps all associations between variables in the residuals. The null hypothesis is that all variables are independent.

The model residuals are typically reported as standardized Pearson residuals. Residuals with absolute values greater than 4 approximate to the two-tailed probability of p less than 0.0001, and absolute values between 2 and 4 approximate to the two-tailed probability of p less than 0.05. A negative residual represents a class combination that was less frequent than expected under the assumption of independence, while a positive residual represents a class combination that was more frequent than expected.

Following the guidelines first proposed by Friendly (1994), the residuals are displayed by blue shading for positive values and red shading with a dashed border for negative values. Residuals with absolute values less than 2 are shaded white, between 2 and 4 are lightly shaded, and greater than 4 are colored dark.

The independence of samples is an important assumption for log-linear models. With spatially contiguous data it is likely that spatial autocorrelation is present and would violate the assumption of independent samples. We estimated that the effects of spatial autocorrelation within our data was limited to distances less than 200 m. To remove the spatial autocorrelation from our 25 m data set we sub-sampled our raster layers using a randomly located grid that selected every 9^{th} pixel; reducing the total number of pixels from 386,137 to 4,793, after excluding no data pixels. If log-linear models were not used, then all raster pixels were used to create the mosaic plot.

The mosaic plots and log-linear models were created in the R programming language using the Visualizing Categorical Data package (R, http://www.r-project.org/; Meyer, Zeileis, & Hornik, 2014). Due to the large sample size the model test statistics were easily significant, and should not be heavily considered. Instead, the model residuals should be used to help understand the direction and relative magnitude of deviations from the expected cell frequencies under independence.

2.6.2. MPB infestation

Comparison with LANDFIRE

MPB infestation results were compared with the five major LANDFIRE classes to understand how the MPB infestation varied by vegetation type at the landscape scale. The comparison was accomplished by graphing the distribution of MPB infestation classes within each LANDFIRE class. The results include the "inconsistent" cover class, which is considered a classification error and was hypothesized to be related to non-coniferous vegetation types, primarily aspen. The generalized shrubland LANDFIRE class was included to assess how the sparse and bare ground classes could be interpreted.

Comparison with aerial detection survey

USDA aerial detection survey data was used to compare how our MPB infestation classes related to observed trends of MPB expansion across the study area. Yearly survey data of MPB infestation extents were reclassified as the initial infestation year: 2009, 2010, 2011 or Uninfected. The data was then separated into the three elevation groups (upper, middle and lower) to allow three coarse resolution comparisons. Within each group we produced a mosaic plot (Hartigan & Kleiner, 1981; Friendly, 1994) to display the relative proportional area of the year of infestation within each of our MPB infestation classes.

2.6.3. Burn severity

Comparison with LANDFIRE

As with the MPB infestation comparison, the burn severity results were compared with the five major LANDFIRE classes to understand how vegetation types interacted with the wildfire at the landscape scale. The comparison was accomplished by graphing the distribution of burn severity classes within each LANDFIRE class. The generalized LANDFIRE shrubland class was used to understand how the proportion of severity levels changed with canopy cover.

Comparison with BARC and RAVG

Our burn severity map was compared to the four class BARC and RAVG burn severity maps (see 2.3.4. Ancillary data layers). To understand how the class distributions differed between the three maps we opted to create three mosaic plots, one for each possible comparison. For each comparison, areas where either one had no data (e.g. missing scan lines, clouds) were excluded in addition to areas falling outside of the fire perimeter.

Comparison of burn severity metrics

To help understand the comparison of our burn severity map with the BARC and RAVG maps we compared how some of the different input metrics for the three burn severity maps related to each other. The BARC dNBR image was compared with the RAVG RdNBR image to examine how the "relative" modification influences the dNBR metric. To measure the importance of the pre-fire NBR image, we compared the BARC pre-fire NBR image with the BARC dNBR image. The BARC dNBR image was also separately compared to the BARC post-fire NBR image and post-fire RapidEye NDVI image, to understand the importance of post-fire images and the benefit of NBR over NDVI.

The BARC and RAVG images were used at their native 30 m resolution while the RapidEye NDVI was resampled to 30 m from the 5 m source image. For each of the four comparisons we calculated the Pearson's correlation coefficient and create density scatter plots for all 30 m pixels that fell within the burn perimeter.

2.7. Disturbance interactions

2.7.1. Understanding the landscape

Before trying to examine the interactions between burn severity and beetle infestation we needed to understand the ecological composition of the landscape and how each disturbance was associated with it. We opted to use aspect-to-north and forest cover class to divide the study area into different land cover classes for which MPB infestation and burn severity might vary.

At a 25 m resolution we classified each pixel within the High Park Fire burn scar into one of nine classes based on the combination of its aspect-to-north class (North, East-West or South) and forest cover class (lodgepole, mixed-conifer or ponderosa). To understand the distribution of the land cover class co-occurrence we created a two-way mosaic plot and applied a log-linear

model of mutual independence to test whether the frequency of their co-occurrence is independent of each other.

2.7.2. MPB infestation occurrence within the landscape

We examined the distribution of our four main MPB infestation classes (dense vegetation, sparse vegetation, early stage MPB and late stage MPB) within the nine land cover classes to understand how MPB infestation varied within the landscape when controlling for aspect-to-north and forest cover. We created a three-way mosaic plot and applied a log-linear model of joint independence to test for an association between MPB infestation and the land cover classes, excluding any associations between aspect-to-north and forest cover.

2.7.3. Burn severity occurrence within the landscape

We also examined the co-occurrence of our four burn severity classes (unburned, low, moderate and severe) and nine land cover classes to understand how the severity varied within the landscape. We created a three-way mosaic plot and applied a log-linear model of joint independence to test for an association between burn severity and the land cover classes, excluding any associations between aspect-to-north and forest cover.

2.7.4. Disturbance co-occurrences within the landscape

With an understanding of how the land cover classes were associated separately with MPB infestation and burn severity, we examined how the MPB infestation and wildfire were associated. We created a four-way mosaic plot and applied a log-linear model of conditional independence to test for an association between burn severity and MPB infestation, while controlling for each of their separate joint associations with aspect-to-north and forest cover.

3. RESULTS

3.1. Photo interpretation

3.1.1. MPB infestation

After removing poor quality plots (e.g., intersected roads, cloud cover, deciduous trees), there was a total of 355 and 397 photo interpretation plots used for training MPB infestation in 2011 and 2012, respectively (Table 3-1). MPB attack represented the smallest class in 2011 with only 38 plots, while the bare ground class represented the smallest class in 2012 with only 55 plots.

The bare ground class primarily consisted of grassland and shrubland areas that lacked observable tree cover. The sparse and dense vegetation class plots lacked substantial MPB attack and were differentiated by having less than or greater than 50% green tree cover, respectively.

Table 3-1. Photo interpretation classes used for modeling MPB infestation and burn severity.

Infestation class	Plot counts (May 2011)	Plot counts (May 2012)	Burn severity class	Plot counts (July 2012)
Bare Ground	56	55	Unburned	142
Sparse Vegetation	77	116	Low	65
Dense Vegetation	184	114	Moderate	43
MPB Attack	38	112	Severe	144

3.1.2. Burn severity

A total of 394 photo interpretation plots were available for the analysis of burn severity (Table 3-1). The unburned and severe classes contained 142 and 144 plots, respectively, which accounted for 73% of all the plots. The remaining 27% of the plots consisted of 65 low severity and 43 moderate severity plots.

3.1.3. Validation against field data

MPB infestation

Relative to the photo interpretation, the field plots had a low omission error of 14.3% (1 plot) for MPB infestation, but a relatively high commission error of 62.5% (Table 3-2) where omission error represents the exclusion of MPB infected plots and commission error represents the misclassification of green vegetation plots as MPB infected . The comparison had an overall accuracy of 83.3% with a moderate kappa statistic of 0.44.

Table 3-2. Confusion matrix of MPB infestation photo interpretation and ancillary field plots.

	Classes	Field data (>20% pre-fire tree mortality)						
		Healthy		High mortality		Total	Comm. error	Prod. acc.
PI	Uninfected	49	(74.2%)	10	(15.2%)	59	16.9%	83.1%
	MPB infected	1	(1.5%)	6	(9.1%)	7	14.3%	85.7%
	Total	50		16		66		
	Omis. error	2.0%		62.5%		Overall acc. =		83.3%
	User acc.	98.0%		37.5%		Kappa =		0.4389

Burn severity

The burn severity comparison resulted in an overall accuracy of 86.6% with a moderate kappa statistic of 0.79 (Table 3-3). There was 100% agreement in identifying unburned plots, while the field data had a 10.5% omission and 14.3% commission error for severely burned plots. For low and moderate severity plots, the field data had omission and commission errors ranging from 36.4% to 62.5%, indicating a high confusion between those classes; this is not fully represented in the overall accuracy due to the smaller sample size of low and moderate severity plots in the field data.

Table 3-3. Confusion matrix of burn severity photo interpretation and ancillary field plots.

	Classes	Field data (% burned)										
		Unburned		Low sev.		Mod. sev.		Severe sev.		Total	Comm. error	Prod. acc.
PI	Unburned	44	(53.7%)	0	(0.0%)	0	(0.0%)	0	(0.0%)	44	0.0%	100.0 %
	Low sev.	0	(0.0%)	3	(3.7%)	5	(6.1%)	0	(0.0%)	8	62.5%	37.5%
	Mod. sev.	0	(0.0%)	2	(2.4%)	7	(8.5%)	2	(2.4%)	11	36.4%	63.6%
	Severe sev.	0	(0.0%)	1	(1.2%)	1	(1.2%)	17	(20.7%)	19	10.5%	89.5%
	Total	44		6		13		19		82		
	Omis. error	0.0%		50.0%		46.2%		10.5%		Overall acc. =		86.6%
	User acc.	100.0 %		50.0%		53.8%		89.5%		Kappa =		0.7871

3.2. Tier-1 classification

3.2.1. MPB infestation

Overall accuracy

The tier-1 MPB infestation classification models had overall accuracies of 93.5% for May 2011 and 92.2% for May 2012 (Figure 3-1a, Table 3-4a & Table 3-5a) and strong kappa statistics of 0.90 and 0.89 (Figure 3-1b). Using cross-validation the overall accuracies dropped to 81.9% and 83.7% with moderate kappa statistics of 0.72 and 0.75, for May 2011 and May 2012, respectively.

Individual class accuracies

Class accuracies for the May 2011 tier-1 MPB infestation ranged between 91.4% and 96.9% for user accuracy and between 81.8% and 98.2% for producers accuracy (Table 3-4a). Class accuracies for May 2012 ranged between 86.9% and 96.0% for user accuracy and between 83.6% and 99.1% for producers accuracy (Table 3-5a). Dense vegetation and sparse vegetation had the largest single class confusion for both years; the lowest producer accuracy was with sparse vegetation for both years.

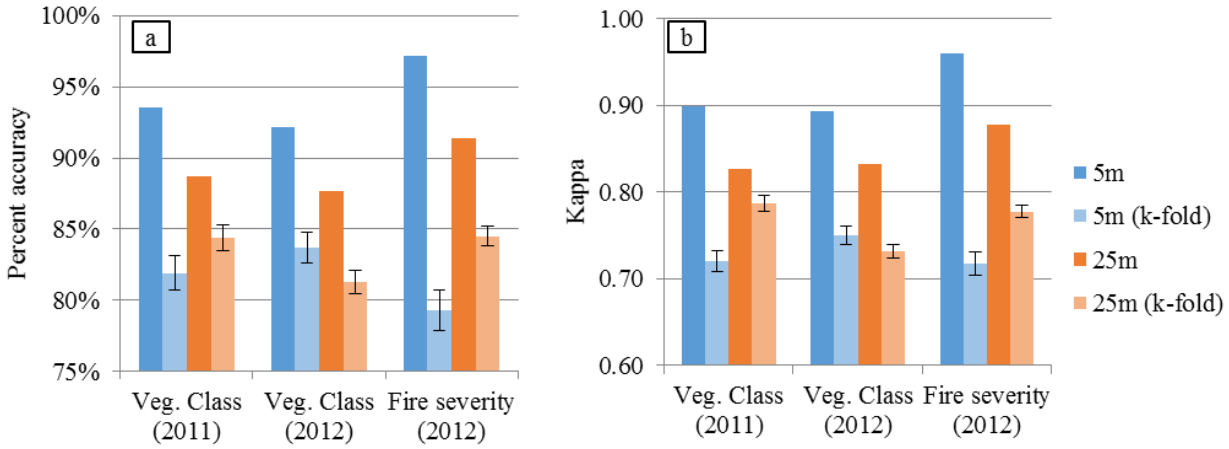

Figure 3-1. Tier-1 and tier-2 classification model summary statistics for all three image dates. (a) Overall class accuracy and (b) kappa statistic.

We examined the uncertainty in class accuracies by comparing the accuracy calculated using all data to the mean of the accuracies obtained from the k-fold analysis. The dense vegetation class for the May 2011 image had the most stable class accuracy (90.1% vs. 88.5%) it also has the most stable user accuracy in May 2012. The MPB attack class had the most stable producer accuracy for the May 2012 k-fold classification model.

In the k-fold analysis for the May 2011 image, the sparse vegetation class user accuracy dropped by the largest margin from 96.9% (for original analysis) to 68.3% (for k-fold analysis). The producer accuracy dropped from 81.8% to 63.7%. For the May 2012 image, sparse vegetation also had the largest drop in user accuracy from 96.0% to 70.7%, while bare ground had the largest drop in producer accuracy from 98.2% to 78.0%.

Attribute usage

The May 2011 tier-1 decision tree utilized the following spectral indices for more than 25% of the plots: Green (100%), NDRE (100%), Red (57%) and NDRRE (30%; Figure 3-2a). The May 2012 tier-2 decision tree primarily utilized: Green (100%), NDRE (100%), NDVI (100%) and RGI (56%).

Table 3-4. Confusion matrices for the May 2011 MPB infestation classifications. (a) Tier-1 and (b) tier-2. K-fold cross-validation is included as an absolute difference from the original.

a. Tier-1, May 2011

	Class	Classification				Total	Prod.	Cross-val.
		Bare ground	Sparse veg.	Dense veg.	MPB attack	(plots)	acc.	diff.
P.I.	Bare ground	55.0 (15.5%)	1.0 (0.3%)	0.0 (0.0%)	0.0 (0.0%)	56	98.2%	-(10.4%)
	Sparse veg.	5.0 (1.4%)	63.0 (17.7%)	8.0 (2.3%)	1.0 (0.3%)	77	81.8%	-(18.1%)
	Dense veg.	0.0 (0.0%)	0.0 (0.0%)	182.0 (51.3%)	2.0 (0.6%)	184	98.9%	-(8.8%)
	MPB attack	0.0 (0.0%)	1.0 (0.3%)	5.0 (1.4%)	32.0 (9.0%)	38	84.2%	-(13.7%)
	Total (plots)	60.0	65.0	195.0	35.0	355		Cross-val.
	User acc.	91.7%	96.9%	93.3%	91.4%	Overall acc. =	93.5%	-(11.6%)
	Cross-val. diff.	-(11.4%)	-(28.6%)	-(4.8%)	-(13.7%)	Kappa =	0.8985	-(0.1785)

b. Tier-2, May 2011

	Class	Classification				Total	Prod.	Cross-val.
		Bare ground	Sparse veg.	Dense veg.	MPB attack	(plots)	acc.	diff.
P.I.	Bare ground	45.0 (12.7%)	11.0 (3.1%)	0.0 (0.0%)	0.0 (0.0%)	56	80.4%	-(0.2%)
	Sparse veg.	4.0 (1.1%)	63.0 (17.7%)	8.0 (2.3%)	2.0 (0.6%)	77	81.8%	-(11.8%)
	Dense veg.	0.0 (0.0%)	4.0 (1.1%)	171.0 (48.2%)	9.0 (2.5%)	184	92.9%	-(2.2%)
	MPB attack	0.0 (0.0%)	0.0 (0.0%)	2.0 (0.6%)	36.0 (10.1%)	38	94.7%	-(11.8%)
	Total (plots)	49.0	78.0	181.0	47.0	355		Cross-val.
	User acc.	91.8%	80.8%	94.5%	76.6%	Overall acc. =	88.7%	-(5.0%)
	Cross-val. diff.	-(12.4%)	-(7.4%)	-(2.9%)	-(2.7%)	Kappa =	0.8272	-(0.0770)

Table 3-5. Confusion matrices for the May 2012 MPB infestation classifications. (a) Tier-1 and (b) tier-2. K-fold cross-validation is included as an absolute difference from the original.

a. Tier-1, May 2012

	Class	Classification				Total	Prod.	Cross-val.
		Bare ground	Sparse veg.	Dense veg.	MPB attack	(plots)	acc.	diff.
P.I.	Bare ground	54.0 (13.6%)	1.0 (0.3%)	0.0 (0.0%)	0.0 (0.0%)	55	98.2%	-(20.2%)
	Sparse veg.	5.0 (1.3%)	97.0 (24.4%)	10.0 (2.5%)	4.0 (1.0%)	116	83.6%	-(15.2%)
	Dense veg.	0.0 (0.0%)	0.0 (0.0%)	113.0 (28.5%)	1.0 (0.3%)	114	99.1%	-(11.8%)
	MPB attack	0.0 (0.0%)	3.0 (0.8%)	7.0 (1.8%)	102.0 (25.7%)	112	91.1%	-(8.1%)
	Total (plots)	59.0	101.0	130.0	107.0	397		Cross-val.
	User acc.	91.5%	96.0%	86.9%	95.3%	Overall acc. =	92.2%	-(12.9%)
	Cross-val. diff.	-(13.0%)	-(25.3%)	-(5.7%)	-(8.9%)	Kappa =	0.8938	-(0.1761)

b. Tier-2, May 2012

	Class	Classification				Total	Prod.	Cross-val.
		Bare ground	Sparse veg.	Dense veg.	MPB attack	(plots)	acc.	diff.
P.I.	Bare ground	53.0 (13.4%)	2.0 (0.5%)	0.0 (0.0%)	0.0 (0.0%)	55	96.4%	-(18.5%)
	Sparse veg.	16.0 (4.0%)	87.0 (21.9%)	11.0 (2.8%)	2.0 (0.5%)	116	75.0%	(1.8%)
	Dense veg.	0.0 (0.0%)	5.0 (1.3%)	108.0 (27.2%)	1.0 (0.3%)	114	94.7%	-(1.5%)
	MPB attack	0.0 (0.0%)	8.0 (2.0%)	4.0 (1.0%)	100.0 (25.2%)	112	89.3%	-(2.7%)
	Total (plots)	69.0	102.0	123.0	103.0	397		Cross-val.
	User acc.	76.8%	85.3%	87.8%	97.1%	Overall acc. =	87.7%	-(3.2%)
	Cross-val. diff.	(3.2%)	-(8.8%)	-(1.2%)	-(4.0%)	Kappa =	0.8329	-(0.0454)

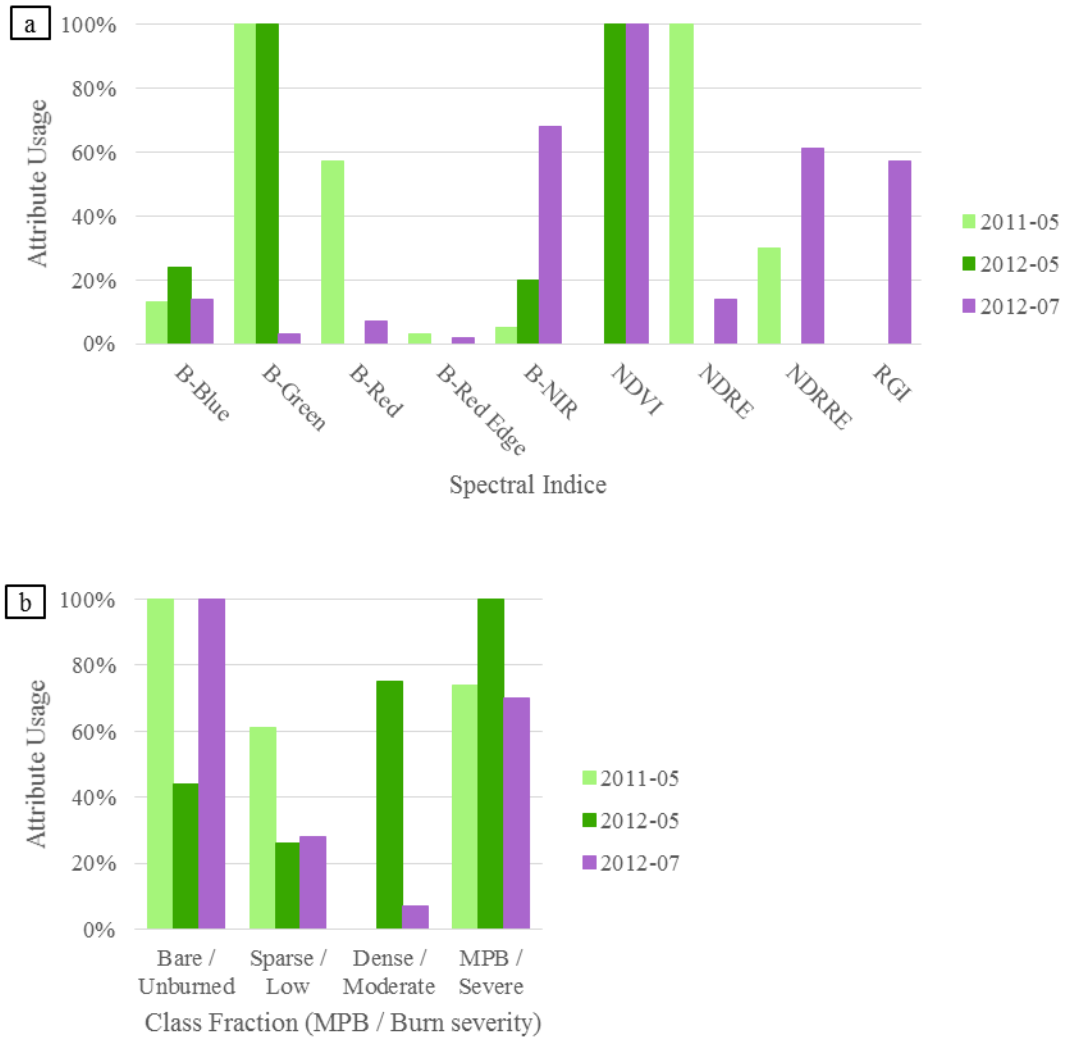

Figure 3-2. Decision tree attribute usage for (a) tier-1 spectral indices and (b) tier-2 class fraction signatures.

3.2.2. Burn severity

Overall accuracy

The tier-1 burn severity classification model produced an overall accuracy of 97.2% with a strong kappa statistic of 0.96 (Figure 3-1, Table 3-6a). Using cross-validation the overall accuracy dropped to 79.3% with a moderate kappa statistic of 0.72.

Table 3-6. Confusion matrices for the July 2012 burn severity classifications. (a.) Tier-1. (b.) Tier-2. K-fold cross-validation is included as an absolute difference from the original.

a. Tier-1, July 2012

	Class	Classification				Total (plots)	Prod. acc.	Cross-val. diff.
		Unburned	Low sev.	Moderate sev.	Severe sev.			
P.I.	Unburned	141.0 (35.8%)	1.0 (0.3%)	0.0 (0.0%)	0.0 (0.0%)	142	99.3%	-(8.2%)
	Low sev.	2.0 (0.5%)	62.0 (15.7%)	1.0 (0.3%)	0.0 (0.0%)	65	95.4%	-(36.8%)
	Moderate sev.	1.0 (0.3%)	2.0 (0.5%)	38.0 (9.6%)	2.0 (0.5%)	43	88.4%	-(35.1%)
	Severe sev.	1.0 (0.3%)	1.0 (0.3%)	0.0 (0.0%)	142.0 (36.0%)	144	98.6%	-(8.3%)
	Total (plots)	145.0	66.0	39.0	144.0	394		Cross-val.
	User acc.	97.2%	93.9%	97.4%	98.6%	Overall acc. =	97.2%	-(15.9%)
	Cross-val. diff.	-(7.8%)	-(34.6%)	-(42.7%)	-(8.0%)	Kappa =	0.9598	-(0.2285)

b. Tier-2, July 2012

	Class	Classification				Total (plots)	Prod. acc.	Cross-val. diff.
		Unburned	Low sev.	Moderate sev.	Severe sev.			
P.I.	Unburned	134.0 (34.0%)	7.0 (1.8%)	1.0 (0.3%)	0.0 (0.0%)	142	94.4%	-(0.4%)
	Low sev.	2.0 (0.5%)	57.0 (14.5%)	5.0 (1.3%)	1.0 (0.3%)	65	87.7%	-(13.7%)
	Moderate sev.	0.0 (0.0%)	7.0 (1.8%)	34.0 (8.6%)	2.0 (0.5%)	43	79.1%	-(28.1%)
	Severe sev.	0.0 (0.0%)	4.0 (1.0%)	5.0 (1.3%)	135.0 (34.3%)	144	93.8%	-(4.0%)
	Total (plots)	136.0	75.0	45.0	138.0	394		Cross-val.
	User acc.	98.5%	76.0%	75.6%	97.8%	Overall acc. =	91.4%	-(6.9%)
	Cross-val. diff.	-(4.8%)	-(8.7%)	-(18.8%)	-(6.4%)	Kappa =	0.8774	-(0.1000)

Individual class accuracies

Class accuracies for tier-1 burn severity ranged between 93.9% and 98.6% for user accuracy and between 88.4% and 99.3% for producers accuracy (Table 3-6a). Where there was class confusion, only 1 or 2 plots were incorrectly classified.

After applying k-fold cross-validation, the unburned and severe severity levels had minimal changes in class accuracies; producer and user accuracies ranged from 89.4% to 91.1%. Low and moderate severity levels had the largest drop in class accuracies when applying k-fold cross-validation. Low severity's user accuracy dropped from 93.9% to 59.3% while producer accuracy dropped from 95.4% to 58.6%. Moderate severity's user accuracy dropped from 97.4% to 54.8% while producer accuracy dropped from 88.4% to 53.3%. The relatively large drop in class accuracies for low and moderate severity levels reveals class confusion at the tier-1, 5 m level.

When the cross-validation reveals a large change in class accuracy, it likely indicates that either the class boundary conditions are under sampled or that there is an issue with capturing the general class signature. In the former case, the smaller training datasets used in cross-validation would produce new class confusion between neighboring classes, while the latter case would increase in class confusion between all classes.

An examination of the tier-1 cross-validation confusion matrix revealed that of the 73.7 plots that were misclassified, only 10.4 plots (14.1%) were misclassifications to non-neighboring classes. Of those plots, 8.2 were due to confusion between low and severe burn, 0.7 were between unburned and severe burn, and 1.5 were between unburned and moderate severity. With the majority of the class confusion coming from neighboring classes (63.3 plots), the cross-validation indicates a possible under sampling of the class boundary conditions at the 5 m level.

Attribute usage

The burn severity tier-1 decision tree utilized the following spectral indices for more than 25% of the plots: NDVI (100%), NIR (68%), NDRRE (61%) and RGI (57%; Figure 3-2a).

3.3. Tier-2 classification

3.3.1. MPB infestation

Class fraction signatures

Class fractions signatures calculated at the 25 m resolution were compared to the single 25 m thematic class assigned by the photo interpretation (Figure 3-3). For May 2011, the 25 m bare ground class was found to be dominated by bare ground pixels (74.2%) with the remaining area primarily sparse vegetation (25.5%; Figure 3-3a). The sparse vegetation class was mostly sparse vegetation pixels (59.2%) with some areas of dense vegetation (24.3%). The dense vegetation class was heavily dominated by pixels of its own class at 86.6%. The MPB attack class was made up of almost half dense vegetation pixels (48.5%) and half MPB attack pixels (43.0%).

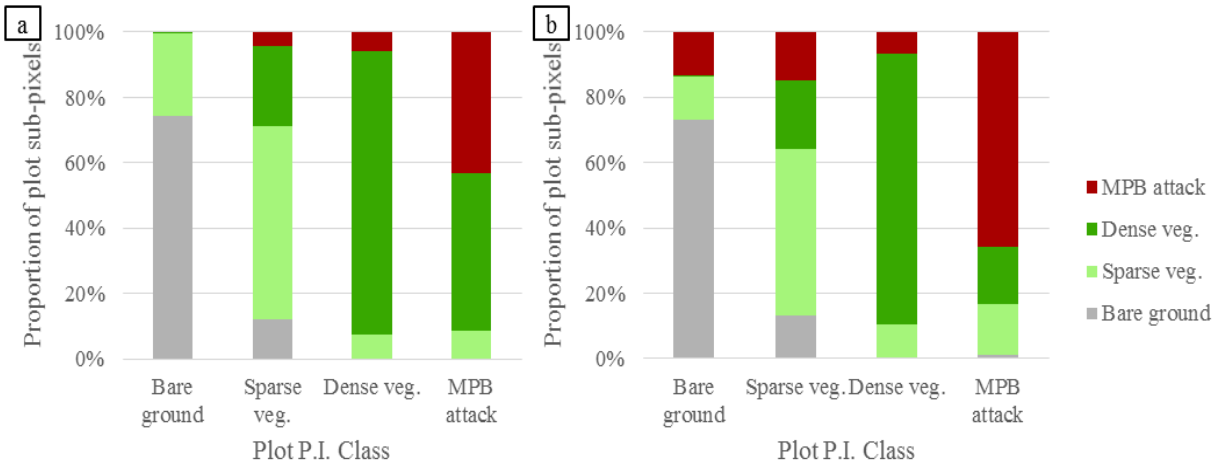

Figure 3-3. Average class fraction signatures for the MPB infestation classifications. (a) May 2011 and (b) May 2012.

For May 2012, the 25 m bare ground class continued to be dominated by bare ground pixels (73.2%), but with the remaining area now being split between sparse vegetation pixels (13.2%) and MPB attack pixels (13.3%; Figure 3-3b). Within the sparse vegetation class, the proportion of sparse vegetation pixels (50.9%) and dense vegetation pixels (20.9%) decreased slightly, while the area of MPB attack pixels (14.9%) increased. The dense vegetation class remained mostly constant between 2011 and 2012 with most of the area being dominated by dense vegetation pixels (82.9%), a slight drop from 2011 that contributed to a slight increase in the amount of sparse vegetation pixels (10.2%) and MPB attack pixels (6.7%). The MPB attack class became dominated by MPB attack pixels with an increase from 43.0% of pixels in 2011 to 66.0% of pixels in 2012, drastically reducing the area of dense vegetation pixels from 48.5% to 15.1%.

Between May 2011 and May 2012 we can see that the largest change is the increase in the area of MPB attack pixels within the bare ground, sparse vegetation and MPB attack thematic classes, indicating an intensification of MPB infestation (Figure 3-3). Between the two dates we observed almost no change in the area of forested pixels (sparse vegetation, dense vegetation and MPB attack) across all thematic classes; the largest change in the area of bare ground pixels was within the sparse vegetation class, from 12.2% of pixels in 2011 to 13.3% of pixels in 2012.

Overall accuracy

Training the tier-2 MPB infestation classification model using class fraction signatures resulted in overall accuracies of 88.7% for 2011 and 87.7% for 2012, and a strong kappa statistic of 0.83 for both years (Figure 3-1, Table 3-4b & Table 3-5b). Using cross-validation the overall accuracies dropped to 84.4% and 81.3% with moderate kappa statistics of 0.79 and 0.73, for 2011 and 2012, respectively.

Individual class accuracies

Class accuracies for the May 2011 tier-2 MPB infestation ranged between 76.6% and 94.5% for user accuracy and between 80.4% and 94.7% for producers accuracy. Class accuracies for May 2012 ranged between 76.8% and 97.1% for user accuracy and between 75.0% and 96.4% for producers accuracy.

Cross validation resulted in lower accuracy statistics for all tier-1 and tier-2 models but the magnitude of the reduction was generally smaller for tier-2 models than for tier-1 models. Seven out of eight (four classes, each with a user and producer accuracy) May 2011 class accuracies had smaller reductions due to the tier-2 cross-validation than the tier-1 cross-validation; the change in user accuracy for bare ground increased slightly from -11.4% to -12.4%. In addition, five class accuracies had absolutely higher values after the tier-2 cross-validation than their respective tier-1 cross-validated accuracies; the exceptions were the user and producer accuracies for bare ground and the user accuracy of MPB attack.

All class accuracies for May 2012 were reduced less after the tier-2 cross-validation than the tier-1 cross-validation. In addition, seven of eight class accuracies had higher values after the tier-2 cross-validation than their respective tier-1 accuracies; the bare ground class was the exception with producer accuracy of 78.0% for tier-1 and 77.8% for tier-2, after cross-validation.

Attribute usage

The decision tree class fraction utilization for May 2011 tier-2 was: bare ground (100%), MPB attack (74%), sparse (61%) and dense (0%; Figure 3-2b). For May 2012, the tier-2 utilization was: MPB attack (100%), dense (75%), bare (44%) and sparse (26%). Note that since the class fractions sum to one, the exclusion of a specific class fraction does not rule out indirect influences on the decision tree.

3.3.2. Burn severity

Class fraction signatures

Burn severity class fraction signatures calculated at the 25 m resolution were compared to the single 25 m thematic class assigned by the photo interpretation (Figure 3-4). The 25 m unburned class was found to be dominated by unburned pixels (85.3%) with small areas of low severity pixels (13.7%). The severe burn class was dominated by severe pixels (74.4%), with most of the remainder being moderate (15.1%) and low (8.9%) severity pixels. Low severity was found to primarily contain low severity pixels (48.2%), while unburned (27.8%), moderate (13.5%) and severe (10.5%) made up a majority of the overall class fraction signature. Moderate burn class was comprised almost equally of moderate (34.2%), low (29.8%) and severe (24.1%) severity pixels.

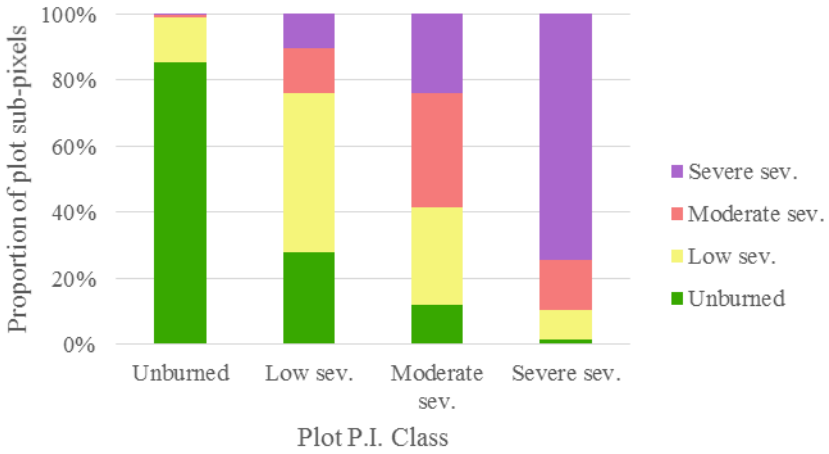

Figure 3-4. Average class fraction signatures for the burn severity classification.

Overall accuracy

Training the tier-2 burn severity classification model using class fraction signatures resulted in an overall accuracy of 91.4% and a strong kappa statistic of 0.88 (Figure 3-1, Table 3-6b). Using cross-validation the overall accuracy dropped to 84.5% with a moderate kappa statistic of 0.78.

Individual class accuracies

Class accuracies for tier-2 burn severity ranged between 75.6% and 97.8% for user accuracy and between 79.1% and 94.4% for producers accuracy. All class accuracies for July 2012 were reduced less after the tier-2 cross-validation than the tier-1 cross-validation. In addition, six class accuracies had higher values after the tier-2 cross-validation than their respective tier-1 accuracies; the exceptions were the producer accuracies for moderate (from 53.3% to 50.9%) and severe (from 90.3% to 89.8%).

Similar to the tier-1 classification model, the low and moderate severity levels had the largest drop in class accuracies when applying cross-validation. Producer accuracy dropped to 74.0% and 50.9%, for low and moderate, respectively; user accuracy dropped to 67.3% and 56.7%, respectively; an improvement over the tier-1 model in three of four cases.

While the average number of non-neighboring plots that were misclassified during cross-validation remained approximately the same from tier-1 (10.4 plots) to tier-2 (10.5 plots), the number of misclassified neighboring plots decreased from 63.3 plots at tier-1 to 50.7 plots at tier-2. Indicating that while the class confusion is still primarily due to neighboring classes, there is an improvement in the tier-2 classification model's ability to separate neighboring classes.

Attribute usage

Class fraction utilization for the July 2012 tier-2 decision tree was: unburned (100%), severe (70%), low (28%) and moderate (7%; Figure 3-2b).

3.3.3. Data products

MPB infestation over two years

The two MPB infestation maps were combined to produce a single map containing two stages of MPB attack. This resulted in five primary classes that covered approximately 97.1% of

the HPF burn scar (Figure 3-5). The percent acreage of the primary classes was: bare ground (13.3%), sparse vegetation (32.0%), dense vegetation (34.7%), early stage MPB attack (12.7%) and late stage MPB attack (4.4%). Within the early stage MPB attack class, 13.0% of it had missing or obstructed imagery for May 2011, and could be considered in an unknown stage of MPB attack; we have treated it as early stage MPB attack to prevent the overestimation of late stage MPB attack.

The remaining 2.9% of the HPF burn scar was comprised of "inconsistent" cover class combinations caused by non-targeted land cover classes (e.g. urban areas, agriculture lands, deciduous trees) or classification error. The following unexpected combinations covered greater than 0.1% of the burn scar: bare ground to MPB attack (0.3%), MPB attack to sparse vegetation (1.5%) and MPB attack to dense vegetation (1.2%). A qualitative inspection of the maps revealed that a moderate portion of the inconsistent class pixels were clumped together in a few areas that appeared to green up between images, which may be mixed stands of aspen and conifer trees that weren't identified earlier.

Burn severity

The July 2012 tier-2 classification model was used to produce the final 25 m burn severity map containing four severity classes (Figure 3-6). The percent acreage for those classes were: unburned (12.8%), low (27.5%), moderate (18.7%) and severe (41.0%).

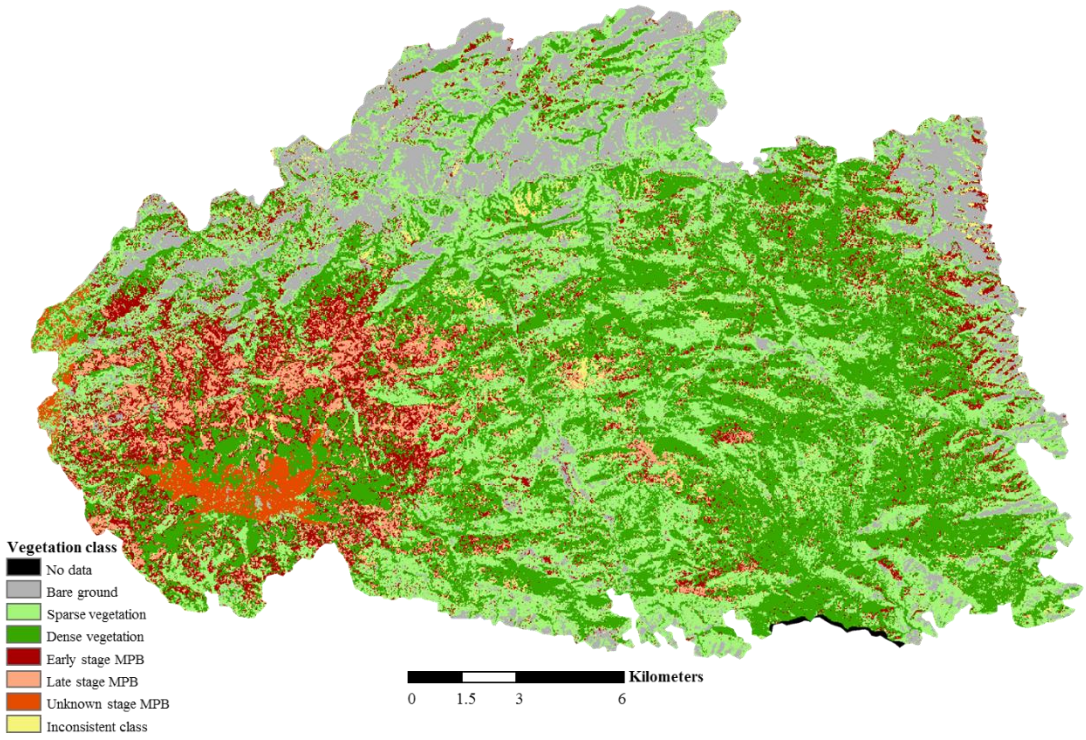

Figure 3-5. Classified map of MPB infestation, covering the two years prior to the HPF, created using the May 2011 and May 2012 tier-2 classification models (25 m).

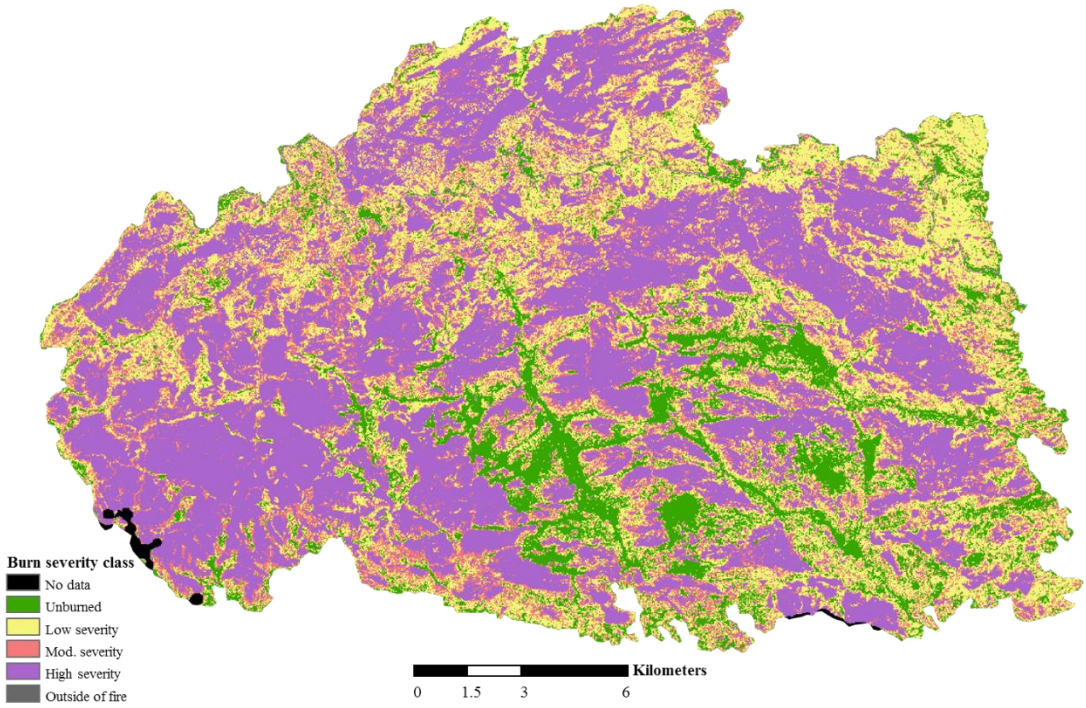

Figure 3-6. Classified map of burn severity created using the July 2012 tier-2 classification model (25 m).

3.4. Comparison with ancillary data

3.4.1. MPB infestation

Comparison with LANDFIRE

Five main LANDFIRE vegetation classes dominate the HPF burn scar, covering 91.4% of its acreage (Figure 3-7). The three conifer forest types each contained approximately the same total acreage of MPB attack; 1,800 ha of early and late stage MPB, each. However, because the total area of each forest type varies, roughly 51.4% of the lodgepole stands were classified as either stage of MPB attack, while only 16.5% of the mixed conifer stands and 11.7% of the ponderosa stands were classified as MPB. In addition, lodgepole stands contained almost no bare ground acreage and the least amount of sparse vegetation relative to its total acreage. Shrubland was found to contain the highest relative proportion and total area of the bare ground class (63.3%; 2,083 ha), with a majority of the remaining area being sparse vegetation (31.4%).

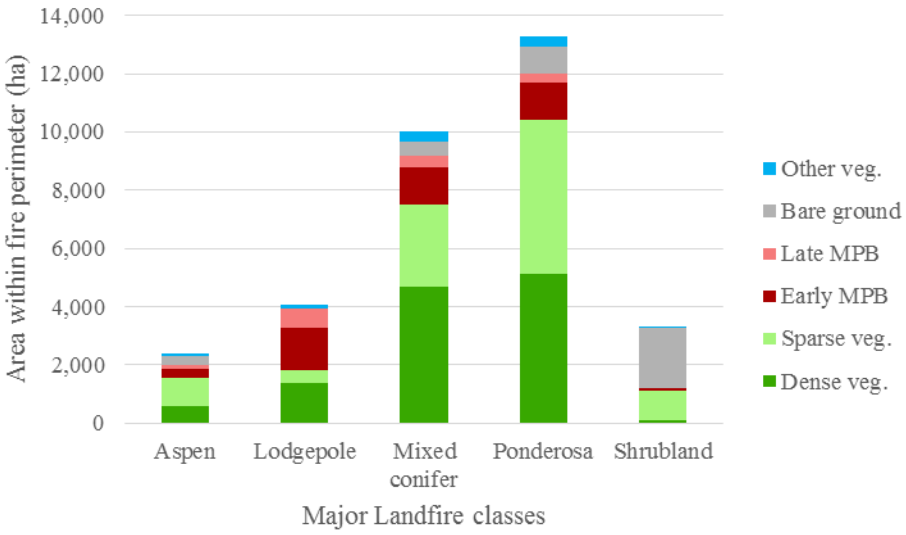

Figure 3-7. Acreage of the five major LANDFIRE vegetation types. Each vegetation type is broken down into the acreage of each MPB infestation class.

Comparison with aerial detection survey

According to the USDA aerial detection survey data, a majority of the higher elevation areas were first attacked by MPB in 2009, while the lower elevation areas were attacked a year later (Figure 2-3, Figure 3-8). While the survey data was able to capture the landscape scale trend, our vegetation and MPB classification results indicate that the survey is unable to capture the forest patch scale; for example, our map indicates that 41.4% of the upper elevation acreage contained MPB infestation, while the survey data reports 94.2% as MPB infestation.

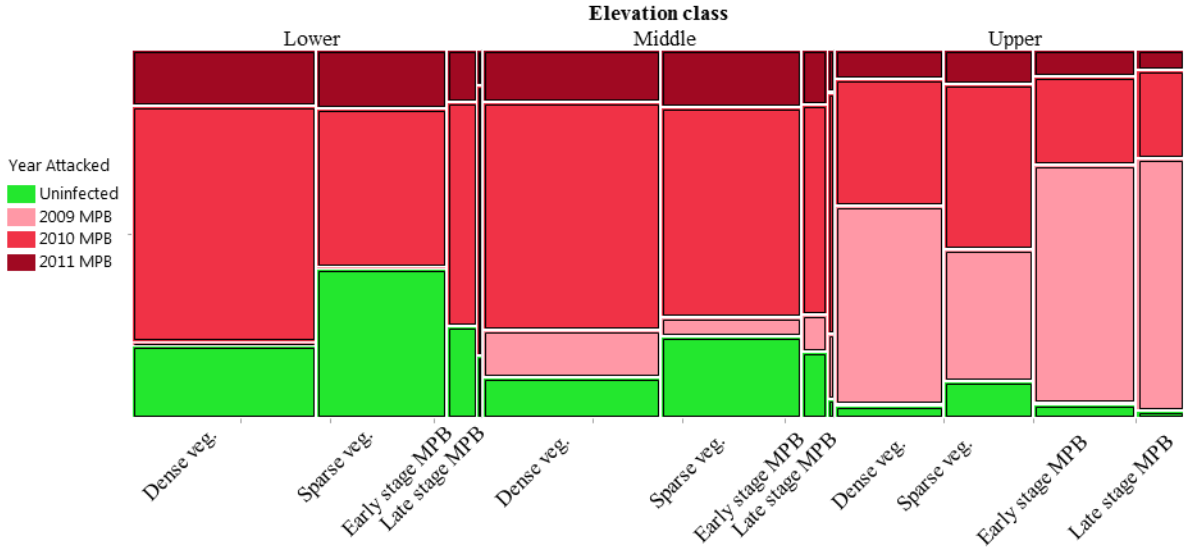

Figure 3-8. Mosaic plot of MPB attack year (USDA aerial detection survey) and MPB infestation class, within three major elevation categories. The width of each rectangle represents the relative area of the vegetation class within its elevation category; the height represents the relative area of each MPB attack year within each vegetation class.

3.4.2. Burn severity

Comparison with LANDFIRE

Of the five major LANDFIRE vegetation classes, lodgepole pine forests contained the highest relative amount of severely burned area at 69.2% (Figure 3-9), followed by mixed conifer (49.7%) and ponderosa pine forests (39.6%). Ponderosa had the highest relative

proportion of unburned, low and moderate severity of the three conifer forest classes. Shrubland areas were mostly dominated by unburned and low severity (23.8% and 45.9%, respectively), while aspen experienced an almost equal mix of the four burn severity classes.

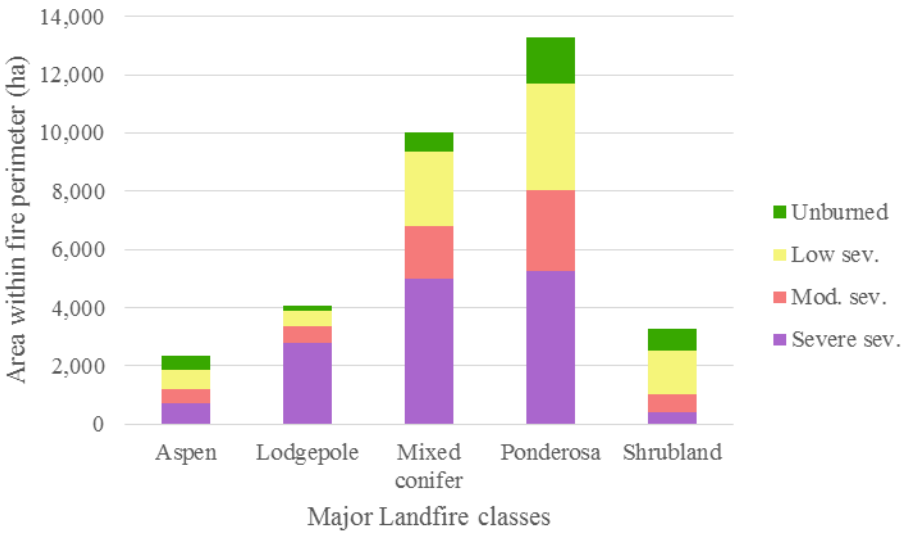

Figure 3-9. Acreage of the five major LANDFIRE vegetation types. Each vegetation type is broken down into the acreage of each burn severity class.

Comparison with BARC and RAVG

Comparing the BARC map against our burn severity map reveals a very low commission error of 2.3% for the BARC severe class, but a very large omission error of 72.3% for the BARC map (Figure 3-10a). In part due to the large severe class omission error, the BARC map also has a very large commission error of 78.2% for its moderate severity class. Overall the two maps have a 42.8% agreement rate.

Alternatively, comparing our burn severity map against the RAVG map resulted in a lower omission error of only 6.3%, but a higher commission error of 24.2% for RAVG's severe class (Figure 3-10b). Similar to the BARC comparison, low and moderate severity levels had high commission and omission errors. Overall the RAVG map had a slightly higher agreement rate of 62.7%.

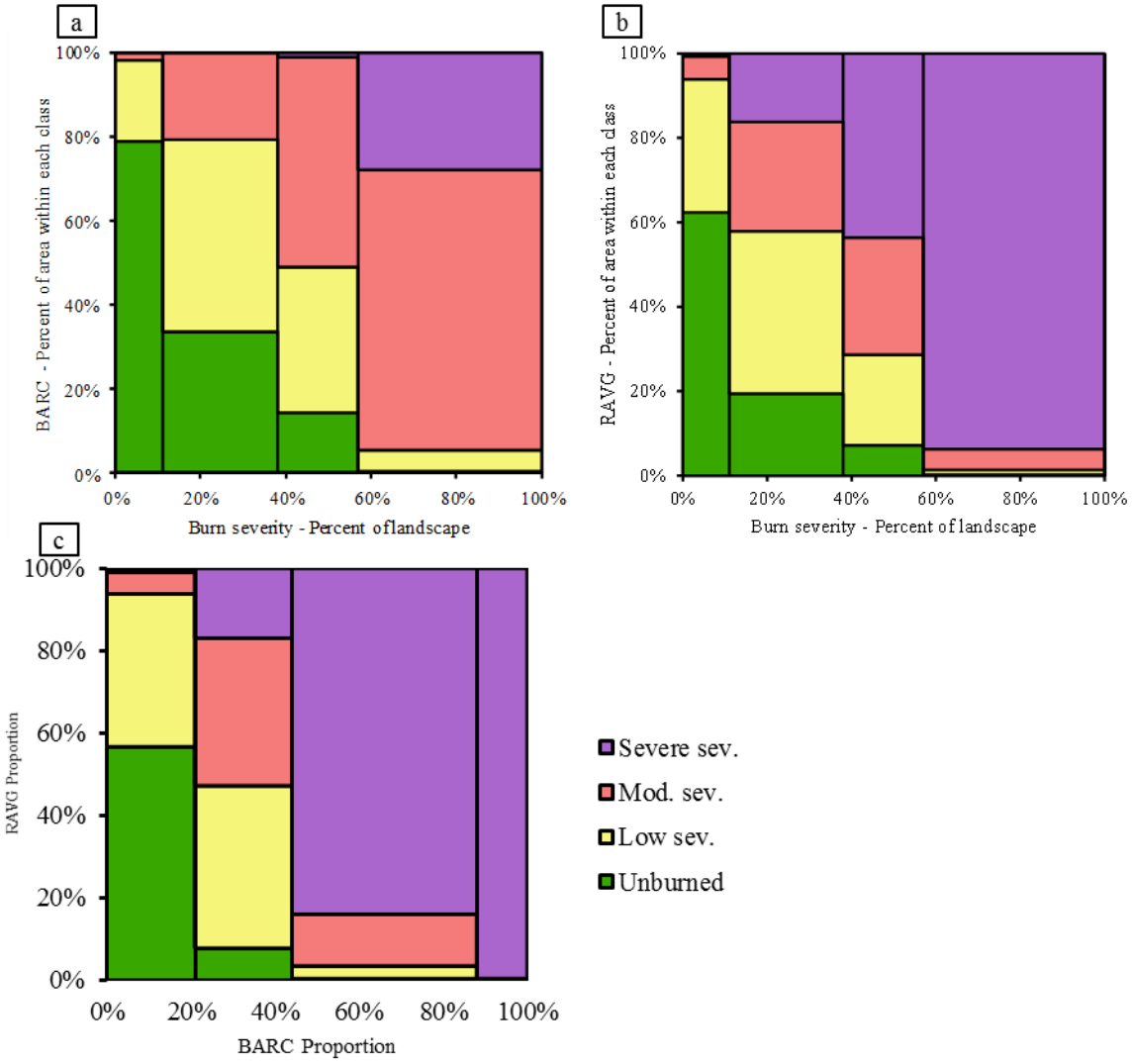

Figure 3-10. Mosaic plots of burn severity map comparisons. (a) BARC vs. our burn severity, (b) RAVG vs. our burn severity, and (c) RAVG vs. BARC.

Comparing the BARC map against the RAVG map reveals a similar pattern where the overall agreement rate is even lower at 38.5% (Figure 3-10c).

Comparison of burn severity metrics

The correlation of the BARC dNBR image with the RAVG RdNBR image was 0.88 (Figure 3-11a); the distribution of both metrics was slightly bi-modal, producing two main groupings of values within the scatter plot, where the grouping at a higher burn severity scale had a shallower slope. Comparing the BARC pre-fire NBR with the dNBR image resulted in a

correlation of 0.41 (Figure 3-11b). Within the scatter plot there appears to be a poor correlation of low dNBR values (lower levels of burning) with pre-fire NBR, but a high positive correlation at higher dNBR values. Post-fire NBR had a negative correlation of -0.85 with dNBR (Figure 3-11c), where most post-fire NBR values were located at low NBR values. Post-fire NDVI had a negative correlation of -0.68 (Figure 3-11d); compared to post-fire NBR, the distribution of NDVI was closer to normal.

3.5. Disturbance interactions

3.5.1. Understanding the landscape

The test of mutual independence between aspect-to-north and forest cover was rejected, indicating an association between the layers ($p < 0.0001$). Lodgepole pine stands comprised the smallest forest cover class and did not produce significant model residuals for any aspect-to-north class combination (Figure 3-12a). Mixed-conifer had significantly more north facing stands and significantly fewer south facing stands than expected. Ponderosa pine was the largest forest cover class and had significantly fewer north facing stands and significantly more east-west and south facing stands. Although all ponderosa class combinations were significant, the mosaic plot (Figure 3-12a) reveals that it was comprised of almost equal proportions of aspect-to-north classes. Due to the high association of north facing slopes and mixed conifer stands, the expected proportions of north facing stands for all forest classes was greater than one-third (Figure 3-12b).

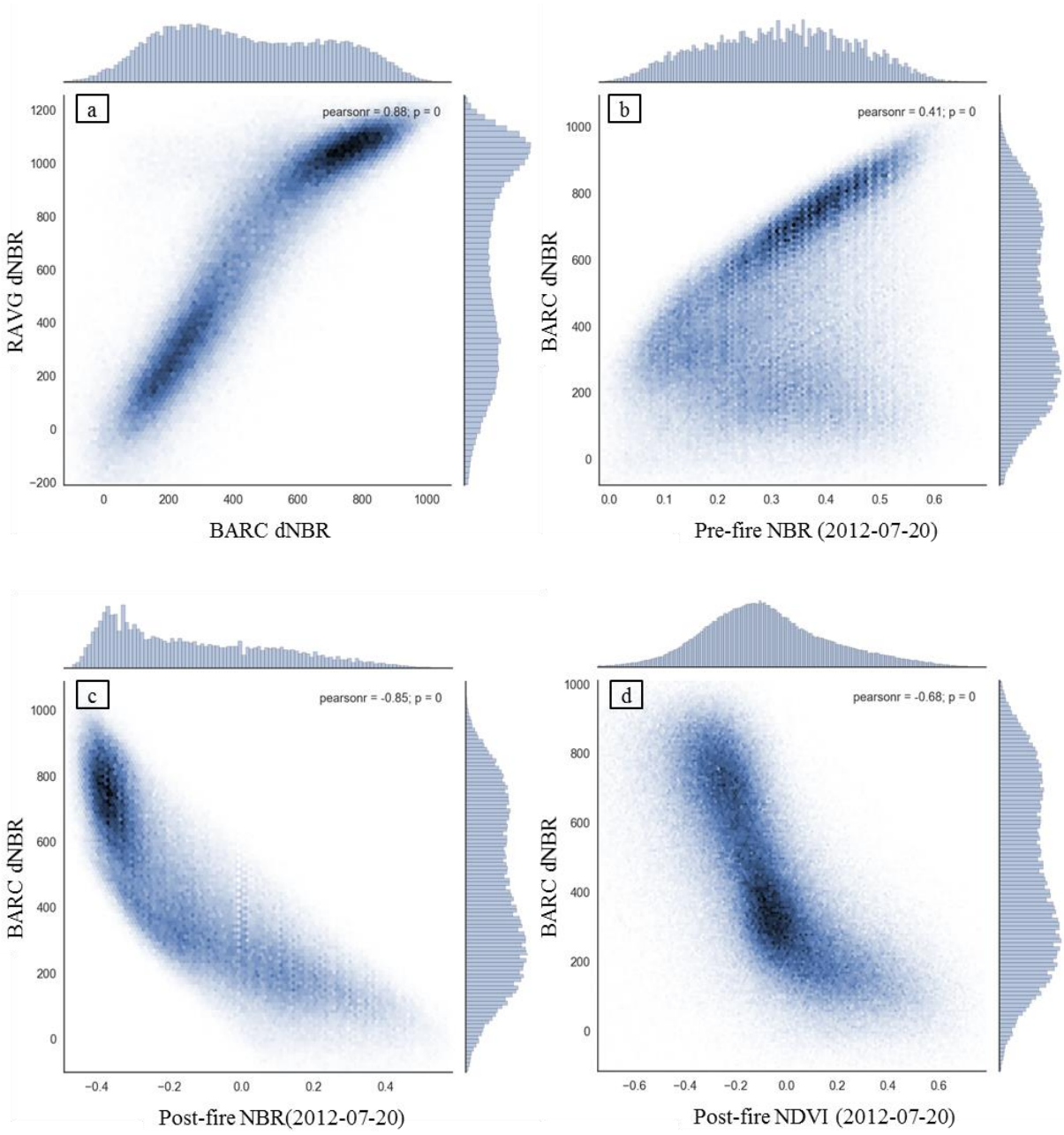

Figure 3-11. Scatter plot comparisons of burn severity metrics. (a) BARC dNBR vs. RAVG RdNBR, (b) pre-fire BARC NBR vs. BARC dNBR, (c) post-fire BARC NBR vs. BARC dNBR, and (d) post-fire RapidEye NDVI vs. BARC dNBR.

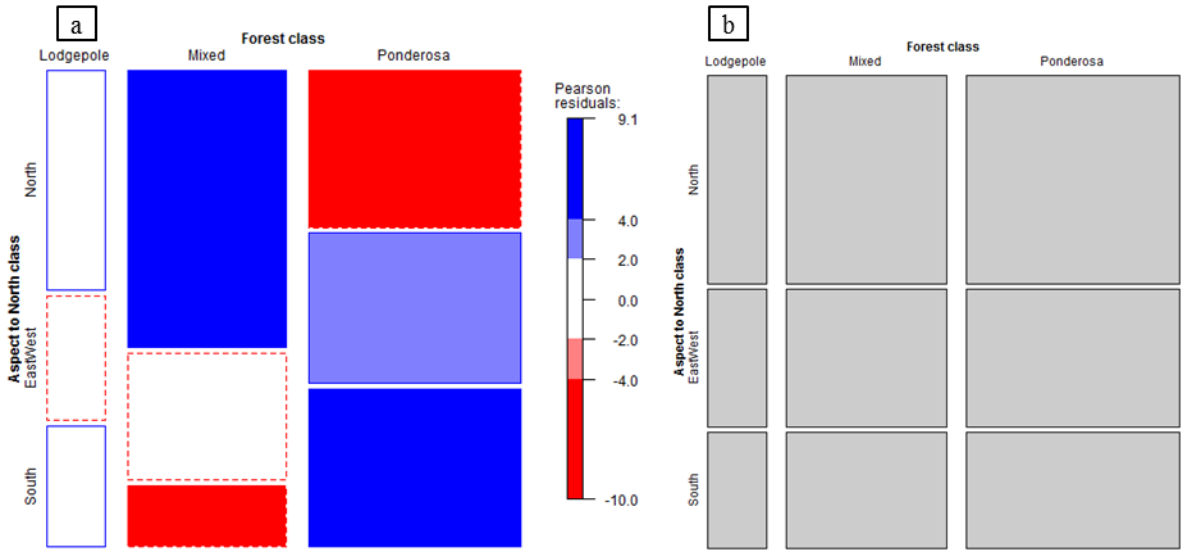

Figure 3-12. Mosaic plot displaying the mutual independence of forest cover and aspect-to-north. (a) Observed frequencies and (b) expected frequencies under independence.

3.5.2. MPB infestation occurrence within the landscape

Controlling for the associations found within the land cover classes (Figure 3-12a), we rejected the test of MPB infestation's joint independence ($p < 0.0001$). We found many significant model residuals that indicate a potential association between the MPB infestation and land cover (Figure 3-13a).

Within the lodgepole forest class we found that both stages of MPB infestation (MPB-Early and MPB-Late) were significantly more frequent than was expected across all aspect-to-north classes (Figure 3-13a). Dense north facing lodgepole frequencies were within the expected range while sparse north facing lodgepole was almost zero, which was significantly less than expected. Dense and sparse lodgepole combinations of east-west and north facing were all significantly less frequent than expected. The residuals within the lodgepole class indicates a trend of having a greater composition of MPB infestation, regardless of aspect, relative to the entire landscape.

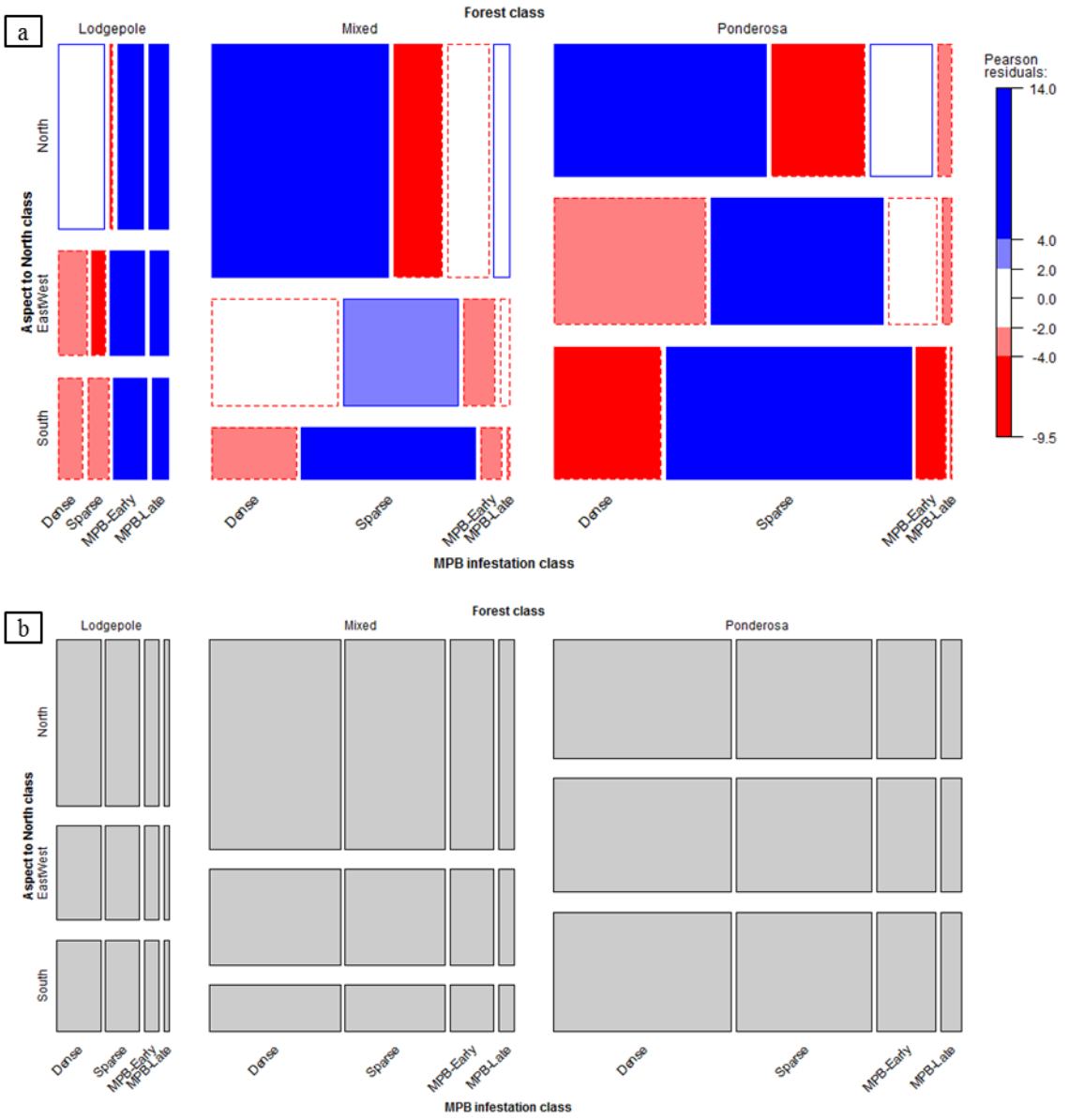

Figure 3-13. Mosaic plot displaying the joint independence of MPB infestation from forest cover and aspect-to-north. (a) Observed frequencies and (b) expected frequencies under independence.

The mixed-conifer forest class residuals for three of the six MPB related class combinations were moderately significant with frequencies less than expected (Figure 3-13a). North facing mixed-conifer stands had significantly more dense vegetation and significantly less sparse vegetation than expected. The opposite was found for south facing stands, where dense vegetation was significantly less and sparse vegetation was significantly more, almost

dominating the class composition. East-west facing stands fell between north and south facing with dense being non-significant and sparse significantly more than expected, but less than within south facing stands. Mixed-conifer stands had a clear association of aspect-to-north and forest cover, with areas of high sparse vegetation having lower than expected amounts of MPB infestation.

The ponderosa pine forest class had a similar trend of residuals as mixed-conifer forest, where aspect-to-north is clearly associated with forest cover, but with more significant residuals than was found within mixed-conifer (Figure 3-13a). Ponderosa did differ in that all aspect-to-north class combinations of MPB-Late were significantly less than expected.

3.5.3. Burn severity occurrence within the landscape

Controlling for the associations found within the land cover classes (Figure 3-12a), we rejected the test of burn severity's joint independence ($p < 0.0001$). We found many significant model residuals that indicate a potential association between burn severity and land cover (Figure 3-14a).

Lodgepole pine stands that were north facing had significantly more severe burn but significantly less moderate and low severity burning. East-west stands were similar but had significantly less unburned stands while moderate severity was not significant. South facing stands were only significant for low severity, which was less than expected. The general trend for lodgepole stands was a higher proportion of severe burn associated with north facing stands and less non-severe burning across all aspect classes.

North facing mixed-conifer stands had significantly more severe burn with significantly less moderate severity and unburned stands than expected. East-west facing stands had significantly more moderate and low severity stands and significantly less unburned. South

facing stands had significantly more low severity with significantly less severe burn. In general mixed-conifer stands had a trend of more severe burn in north facing stands and less severe burning in east-west and south facing stands.

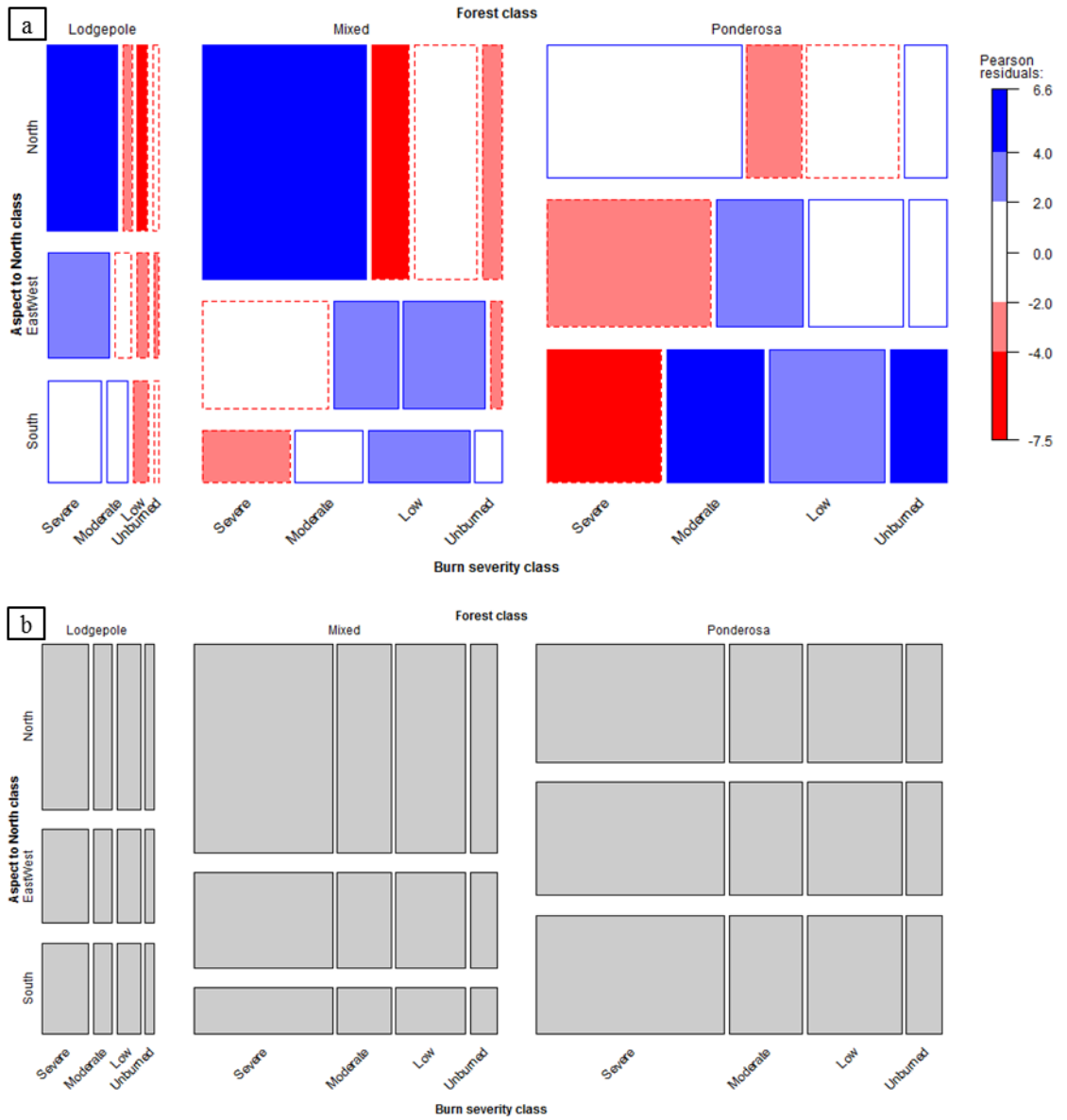

Figure 3-14. Mosaic plot displaying the joint independence of burn severity from forest cover and aspect-to-north. (a) Observed frequencies and (b) expected frequencies under independence.

Ponderosa stands had a positive, but not significant, residual for severe burn within north facing stands, but had significantly less moderate burning. East-west facing stands had

significantly less severe burn but significantly more moderate burning than expected. South facing stands were significant for all severity classes with severe being less than expected while moderate, low and unburned were more frequent than expected. Unlike the other forest classes, ponderosa did not have a significant trend of severe burn in north facing stands, but did have a larger trend of less burning within south facing stands Figure 3-14a.

3.5.4. Disturbance co-occurrences within the landscape

The conditional independence of burn severity and MPB infestation was tested after controlling for the association between the land cover classes (Figure 3-12a) and the separate associations of MPB infestation and burn severity to the land cover classes (Figure 3-13a; Figure 3-14a). We rejected the null hypothesis of conditional independence ($p < 0.0001$). While we found trends within the model residuals that might suggest an association, the lack of significant residuals should be noted (Figure 3-15a). We did not find a major significant trend between MPB infestation and burn severity within lodgepole stands.

For mixed-conifer stands we found that north facing dense stands were left unburned significantly more than expected while sparse was significantly less unburned. East-west facing stands had significantly less severe burn and significantly more moderate burning within sparse vegetation. Although not significant, across all aspect classes, both MPB-Early and MPB-Late had positive residuals for severe burn combinations, indicating a possible association.

Dense vegetation within south facing ponderosa stands had significantly more severe burn and significantly less low severity; conversely, sparse vegetation had significantly less severe burn and significantly more low severity. East-west facing stands of sparse vegetation also had significantly less severe burn than expected. Early stage MPB infestation within east-west facing ponderosa stands had significantly more severe burn.

Looking at the entire mosaic plot (Figure 3-15a), eight of the nine severe burn and dense vegetation combinations had a positive residual, with one significant, while all nine severe burn and sparse vegetation combinations had a negative residual, with three significant.

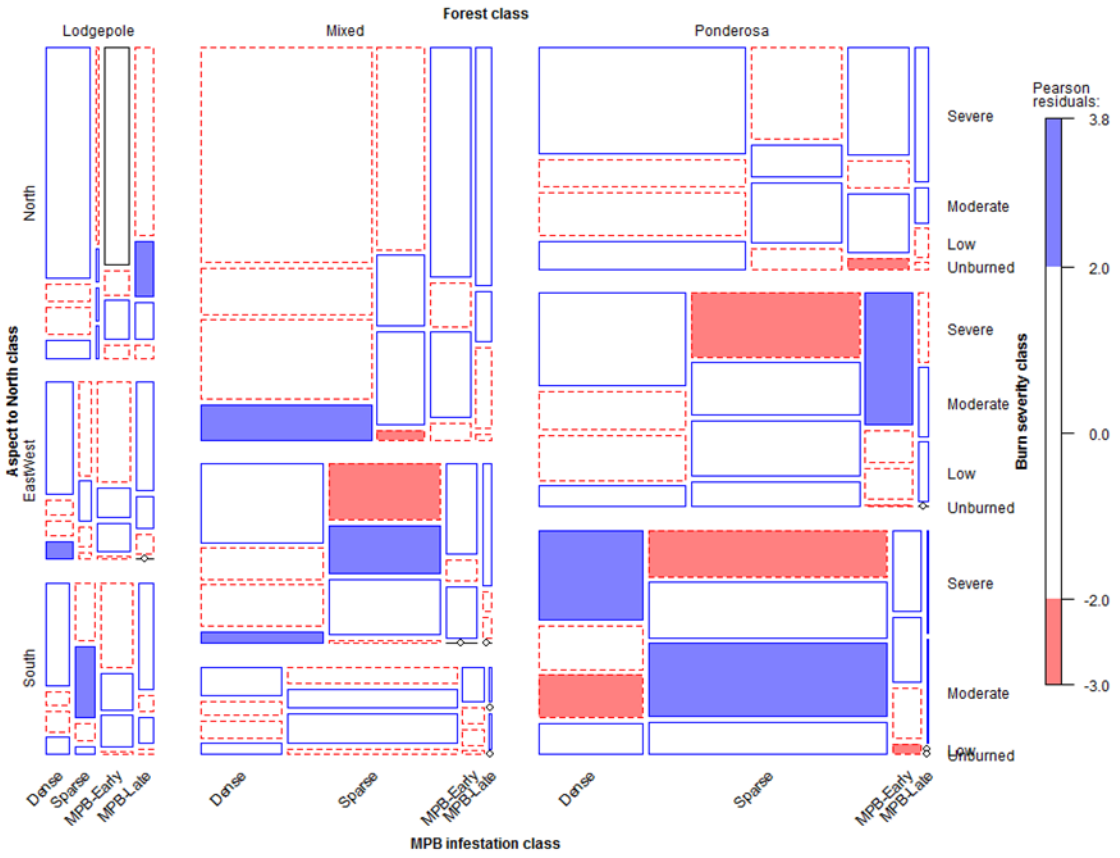

Figure 3-15. Mosaic plot displaying the conditional independence of MPB infestation and burn severity, given forest cover and aspect-to-north.

4. DISCUSSION

4.1. Classification methods

4.1.1. Training data

The methods presented in this paper offer a novel approach to mapping MPB infestation and burn severity at a high and moderate resolution. We found that photo interpretation is a valuable source of training data that scales from forest stands to landscape scales, costs less than field surveys, and can be collected quickly.

MPB infestation

The collection of MPB infestation training data is temporally sensitive due to the rapid transition into the red attack stage and continued loss of needles as the trees reach the grey stage over the following two to three years. We addressed this issue by utilizing a high resolution imagery platform with a constellation of matching sensors that regularly collect scenes, and enable a quick response to ecological disturbances.

Our methods focused on the photo interpretation of plots instead of single pixels because early testing revealed a higher classification error and interpreter bias when attempting to photo interpret a single 5 m pixel; distinguishing between MPB attack and bare ground pixels was the largest source of this error, primarily in areas of sparse vegetation cover or low intensity MPB infestation. Testing also showed that photo interpreting areas greater than 0.1 ha was not suitable for identifying classes of MPB infestation as it would have resulted in an overestimation of MPB area. We opted to use 725 m^2 plots to take advantage of the increased accuracy from interpreting multiple pixels without sacrificing too much spatial detail.

The photo interpretation effort revealed that high intensity MPB infestation was generally clumped into patches; a common characteristic associated with incipient epidemic and epidemic states of MPB infestation (Wulder et al., 2006). During an initial analysis of randomly located plots, we were required to invest more time in the photo interpretation stage in order to reach the desired sample size of MPB infested plots. Photo interpretation efficiency was increased by switching to stratified random selection for plots; we suggest future implementations of our methods utilize stratified selection to increase the probability of sampling the patches of infestation.

Recent studies have used 30 m Landsat imagery for photo interpreting and classifying MPB infestation (Walter & Platt, 2013). Given our results that a 25 m pixel of MPB attack averages only about 43% of MPB dominated pixels at the 5 m scale, we suggest future studies use imagery with a spatial resolution of 5 m or less for MPB infestation estimation; Meddens and Hicke (2014) had success with using high resolution imagery for creating their reference data, which was then used to train a coarser resolution model to classify Landsat imagery. This approach doesn't allow one to characterize the intensity of infestation as we were able to do here.

For our study, RapidEye imagery cost roughly $850 per 94,542 hectare scene (less than $0.01 per hectare). The benefits of using these images included greater confidence in the photo-interpretation accuracy and an enhanced ability to describe the characteristics of our broad land cover classes and these were key factors in the development of our improved methods for MPB and burn severity mapping. Although publicly available Landsat imagery would have been free, we conclude that RapidEye imagery was a good balance between the cost of even higher resolution imagery (e.g. DigitalGlobe Worldview 3) and the lower spatial resolution of Landsat.

Burn severity

Differenced based burn severity maps (e.g. BARC, RAVG) require a pre-fire and post-fire image, so that static patterns of NIR and MIR reflectance can be removed from the final images. One drawback of this approach is that it makes the assumption that changes in the state of the landscape are only attributable to the wildfire. For the HPF study, the BARC map used a June 8th, 2011 pre-fire image, one year prior to the fire, grouping the last year of MPB infestation with the burn severity assessment. The RAVG map used an August 21st, 2009 pre-fire image, almost three years prior to the fire, grouping almost the entire MPB outbreak with the burn severity assessment. Both maps used post-fire images within approximately a month of full containment. The high correlation of the post-fire NBR image with the dNBR image indicates that there was minimal additional information added with the usage of a pre-fire NBR image. Our burn severity classification approach does not require a pre-fire image, reducing the potential biasing of the pre-fire state of the landscape and enabling the use of imaging platforms that do not regularly collect images of forested areas (e.g., high resolution commercial platforms typically don't collect images of a forest until after a major disturbance event).

A major benefit of RapidEye for image interpretation of burn severity is the ability to train a classification model without field data and a faster turn-around than conducting a field survey. Both the BARC and RAVG maps have the ability to be used without field training, but assumes the area is ecologically similar to their original training data (Miller & Thode, 2007), which can lead to error (Figure 3-10). Although their methods indicate that field measures should be taken to ensure class accuracies, this is often not possible due to limited resources or lack of access to remote areas; e.g. the western portion of the HPF had very limited access after the fire roads washed out shortly following the fire.

Relative to MPB infestation, burn severity required less interpreter effort due to the larger size and distinct boundaries of patches at various levels of burn severity. Low and moderate severity classes primarily occurred as narrow strips between unburned and severely burned areas that didn't dominate a training plot's area. This resulted in the infrequent occurrence of a training plot with conditions that ranged from unburned to severely burned with similar proportions. We were able to capture those transitional areas with our two-tier approach; tier-1 was able to identify 5 m pixels across different burn severities, and tier-2 captured the transitional severity signature at the coarser 25 m resolution, maintaining the class distributions.

The use of patches segmented on the basis of spectral, textural and shape attributes to sample homogeneous areas might improve classification accuracy and reduce interpreter fatigue and bias. For instance, Trimble's eCognition software (http://www.ecognition.com/**)** could be used to segment the study area, and then photo interpret the segmented patches using stratified random sampling. That approach could potentially address the difficulties of plots partially intersecting MPB patches or containing multiple burn severity classes, while the class fraction signatures would scale the irregular patch shapes to a standard square gridding.

4.1.2. Classification method

Decision tree

In contrast to other decision tree methods, the C5.0 classifier allowed us to easily examine the classification rules and understand the distinguishing variables and thresholds for each pixel, enabling a more informed approach to revising the classification.

The tier-1 classification model followed traditional methods for the classification of remotely sensed imagery. Departing from those methods, we chose to apply the tier-1 model at a different resolution than the training data, and then utilized the tier-2 classification model to

achieve a spatial resolution consistent with the training data while reducing classification errors. If we had used a different tier-2 method, such as classifying a 25 m pixel based on the dominant 5 m class, we would have biased the 25 m map towards the most prevalent class.

For the burn severity classification models (Table 3-6), we found that when fit using all the available data, the tier-1 model had an overall accuracy of 97.2%, which is 5.8% higher than the tier-2 model when fit using all available data. However, once k-fold cross-validation was applied to both models, the overall accuracy of the tier-1 model dropped by 15.9% to 81.3%; a large change that indicates over fitting of the tier-1 classification model. The tier-2 classification model dropped by 6.9% to 84.5%, which is both a higher overall accuracy than tier-1 and was less influenced by over-fitting. We believe this is one of the key advantages of our methods.

Cross-validation for all three classification sets resulted in lower over-fitting and better goodness-of-fit statistics for tier-2 than tier-1; this can be seen in the overall accuracy and the kappa statistic (Table 3-4, Table 3-5, & Table 3-6).

Our decision tree methods might be further improved by using class weights, model boosting and spectral decomposition. Class weights could be used to correct for imbalances in class frequency; MPB mortality was the least frequent class for MPB and resulted in the lowest influence during model creation.

During the early development of our methods we tested an alternative approach where the tier-1 classification model was trained using each pixel value separately, instead of averaging plot pixel values together. The resulting teir-1 classifier generally had a lower accuracy, but produced a higher accuracy for the tier-2 classification model, even after cross-validation. It appeared that the modified tier-1 classifier produced a class map that resulted in class fraction signatures with higher class separation, allowing for better class predications at the coarser tier-2

resolution. We did not further pursue this alternative approach due to time restrictions and our incomplete knowledge of the causes of increased accuracy. We hope to explore this idea in more detail in the future.

4.2. Case study of the High Park Fire

4.2.1. MPB infestation

Class definitions

The presence and degree of MPB infestation is characterized flexibly in the various stages of these methods. For the tier-1 analysis, it is treated as the presence or absence of at least 25% MPB mortality in either a plot or 5 m pixel. For the class fractions it is treated as the fraction of a plot (or 25 m pixel) that is classified as having more than 25% MPB mortality. As a consequence, we are left with an uncertainty about the actual cover of MPB at these scales because we do not know the average MPB cover of those pixels that were classified as greater than 25% MPB cover. That ambiguity could be resolved partially by using a 1 m spatial resolution image product in place of the 5 m RapidEye, as one might be more confident in describing a single 1 m pixel as either MPB infested or not, relative to a 5 m pixel. However, field observation of infestation indicates 5 m is a suitable scale for classifying MPB infestation using a binary variable.

While our analysis indicated that a single MPB infestation class at 25 m resolution would result in the best classification statistics, it is possible to further characterize plots or 25 m pixels using the class fractions. The MPB infestation class fraction value varies depending on the time since first attacked, stage of MPB infestation and condition of uninfected trees. For the May 2011 MPB attack training plots, the average MPB attack class fraction was 43.0% and of the 38 plots, 32 (84%) had a value greater than or equal to the original definition of 25% MPB attack

cover (5% quantile of 18%; Figure 3-3). In the following year, the average MPB attack class fraction for MPB attack training plots was 66.0% and of the 112 plots, 107 (96%) had a value equal to or greater than our original definition (5% quantile of 29%).

If MPB was only attacking healthy stands and remained in the same outbreak population state, then we'd expect that the distributions from the two years to be equal. Figure 3-3 clearly displays a positive shift in the 2012 distribution, indicating that the remaining healthy trees in MPB infected stands were being attacked and that the outbreak state was either stagnant or progressing towards an epidemic state; an increase in stand-level MPB infestation is not a characteristic of endemic or post-epidemic population states (Wulder et al., 2006). We believe that the ability to make inferences about the local intensification of MPB infestation is enough to recommend the two tier classification approach.

Two-tier classification model

Within the context of a two tier approach we did not expect or require that the tier-1 classification model classify each plot correctly, because it was trained using average plot signatures that might not fully represent the heterogeneity within a plot. The tier-2 classification model was only necessary to capture the class signatures that represent the thematic classes we aimed to map. By applying the cross-validation to the tier-1 classification model, we can identify the thematic classes that might share class signatures at the plot level, and require more spatial detail to distinguish between them (Table 3-4a, Table 3-5a); the classes were a composite of targeted subclasses (e.g. sparse vegetation is comprised of a few healthy trees and mostly understory vegetation). After classifying at the 5 m pixel-level with the tier-1 classification model and retraining with the tier-2 classification model, we were then able to recapture the class

compositions by using class fraction signatures; reducing class confusion and increasing overall accuracy (Table 3-4b, Table 3-5b).

The remaining class confusion at the tier-2 level can be attributed to the inability to identify distinct boundaries between the logical class transitions. The sparse vegetation class could be expected to have the largest difference in cross-validated accuracies since it is the class with the largest potential class overlap; a plot could be on the boundary of bare to sparse, sparse to dense and sparse to MPB attack. In the same sense, dense vegetation could be expected to be the most stable class as it has limited class overlap; a plot would be expected to transition to sparse before bare and before MPB attack, except in high density areas. Misclassification of MPB infestation with sparse and dense vegetation is likely caused by areas where MPB infestation borders the MPB attack cover threshold.

Initial MPB outbreak

The study site's MPB outbreak began showing significant MPB mortality in the summer of 2009 (Figure 2-3, Figure 3-8), but the May 2011 image we used only captured the outbreak's second year (summer 2010). We attempted to study the initial year, but were unable to do so due to limited imagery and low training data sample sizes. A May 2010 RapidEye image was unusable due to cloud cover; as an alternative a September 2009 image was purchased. Photo interpretation of the September image resulted in approximately 10 plots with greater than or equal to 25% MPB cover, resulting in poor classification model statistics when cross-validation was used.

There were three main issues in identifying initial MPB infestation in the September 2009 image. First, the lower intensity and extent of MPB infestation in the initial year severely reduced the chance of randomly sampling plots with greater than or equal to 25% MPB

mortality. Second, a late summer image capture resulted in greater vegetation cover than our May images, making it more difficult to clearly identify MPB mortality in mixed class patches. Lastly, using images from different seasons might have led to the complication of class definitions when incorporating them into a time-series map.

Comparison with field data

The field data provided an independent data set for field based validation of our results. While the two datasets characterized the field plots in different ways (proportion of stems for the field data and proportion of plot area for our analysis) we opted to include this comparison for completeness. Possible sources of error include: sampling different plots due to poor GPS accuracy or poor geolocation of imagery, the inclusion of fallen timber or standing snags that are unobservable with photo interpretation, the lack of field based absolute measures of vegetation cover, limited sample size and differing plot dimensions.

The comparison of the field based percent pre-fire tree mortality against the MPB infection status from photo interpretation found a relatively high agreement for uninfected plots, but lacked an agreement with MPB infection plots (Table 3-2). An examination of the field data and all available imagery indicates that a majority of the field data's omission of MPB could be related to the inclusion of pre-fire tree mortality that is unobservable in the imagery (e.g. lower canopy trees, standing or fallen snags). In addition, the omission of MPB attack in the PI could be explained by field identification of green-attack trees, although the current field data comparison does not appear to indicate that as a major contributor (Table 3-2).

Comparison of beetle infestation with forest type and aerial survey

Within the five main LANDFIRE classes, lodgepole stands contained minimal areas of bare ground or sparse vegetation classes, indicating a higher connectivity between trees and

possibly a higher stand density (Figure 3-7). The lack of any major MPB infestation or dense vegetation in the shrubland class was an expected outcome for this vegetation cover type. The aspen cover class was hypothesized to be a major contributor to the "inconsistent" cover classes, but given that all vegetation classes contained a similar relative proportion of aspen, that hypothesis does not appear to be true; within targeted vegetation cover types, the "inconsistent" class can be interpreted as misclassification error or noise.

The USDA aerial detection survey data did not provide the necessary accuracy for studying MPB infestation at the scale of wildfire patches (Figure 3-8). The main benefit of the survey data is that it is a spatially and temporally complete data set. Its main drawback is the coarse resolution and low accuracy.

Our MPB infestation map and the survey data both found that at the landscape scale, the western portion of the burn scar was attacked a year prior to the eastern portion, but they disagreed in the specific spatial location and rate of MPB infestation. For the western upper-elevation areas, the survey data provides little detail as a majority of the area is marked as MPB infestation from 2009 (the initial year) through 2011 (last pre-fire year; Figure 2-3). A major difference between our maps is that we focused on areas with greater than 25% MPB mortality, while the survey focuses on presence or absence (USDA Forest Service, 1950).

4.2.2. Burn severity

Class definitions

Examination of the class fraction signatures for the original photo interpreted plots revealed that only the unburned and severe classes align with a single dominate photo interpretation definition (Figure 3-4). While the low and moderate classes typically held the largest class fraction signature for their respective plots, they averaged only 48.2% and 34.2% of

the pixels within their respectively thematic classes, indicating the importance of the other classes. This supports the idea that, at the plot-level, low and moderate severity are typically a transitional boundary class where low severity surrounds unburned areas and moderate severity surrounds severe areas, rather than homogeneous patches of similar burn conditions; matching our observations from the photo interpretation work.

Two-tier classification model

By applying cross-validation to the tier-1 classification model, we can see that there was some confusion from assigning a single class to the low and moderate plots (Table 3-6a); at the plot-level a single set of average spectral statistics was unable to capture the transitional properties of the classes. After applying the tier-1 classification at the 5 m pixel-level, we were then able to capture the transitional properties of low and moderate severity classes by using 25 m class fraction signatures; reducing class confusion and increasing overall accuracy (Table 3-6b). On the basis of our training data resolution and resulting transitional definitions of low and moderate severity, the 25 m spatial resolution was a more appropriate choice than 5 m. Using the two-tier approach reduced model over-fitting (smaller changes in class accuracies) and increased the classification model accuracy of burn severity.

Comparison with field data

The field data also provided an independent data set for field based validation of our burn severity results. As with the MPB infestation comparison, the two datasets characterized the field plots in different ways. The field data described burn severity as the wildfire's impact to individual plot stems, while our photo interpretation classes described the areal impact of the wildfire. With those differences, the possible sources of error include: sampling different plots due to poor GPS accuracy or poor geolocation of imagery, the inclusion of fallen timber or

standing snags that are unobservable with photo interpretation, limited sample size, differing plot dimensions and differences in the burn severity class definitions (e.g. whether a tree that was killed by MPB before the fire could be considered severely burned). The high class confusion of low and moderate severity plots was expected since the field data lacked a metric to distinguish these two classes as defined in our photo interpretation (Figure 3-3); the field data only recorded the status of tree mortality, regardless of crown consumption.

Comparison of burn severity maps

We defined our burn severity classes in an explicit manner but a categorical burn severity classification is inherently arbitrary and can be difficult to interpret (Miller & Thode, 2007). There are now three different burn severity maps for the HPF; the BARC map is targeted at impacts on soils, while the RAVG map and our burn severity map are targeted at impacts on vegetation (USDA Forest Service, 2013).

The availability of different burn severity maps leads us to the question of whether there is a quantitatively superior map, or whether the subjective matter of class definitions is the main differentiating factor. Differences between categorical burn severity maps can arise from either identifying different class boundaries of a similar process, or by mapping different processes. In practice, different class boundaries are quite possible due to methods having different default thresholds, target different impacts, or how they are adjusted for each wildfire. Differences in processes may arise by design (e.g., soil vs. vegetation) or through errors (e.g., not accounting for MPB mortality when assessing the state of pre-fire vegetation).

A simple subjective class boundary bias might cause classes to have a high error rate in neighboring classes, but only in one direction (e.g. moderate severity extending into low, but low wouldn't extend into moderate). The comparison of our burn severity map with BARC and

RAVG indicates high error rates spanning multiple classes and in both direction along the severity gradient, indicating that a subjective difference in class boundaries is most likely not the cause of the overall high error (Figure 3-10).

4.2.3. Disturbance interactions

When we examined how MPB infestation varied across the land cover classes (Figure 3-13a), we observed a few key trends. Lodgepole pine stands had a higher proportion of MPB infestation than was expected, regardless of the stand's aspect. Mixed-conifer and ponderosa stands had a strong association of higher canopy cover for north facing stands and lower canopy cover for south facing stands. Higher proportions of dense vegetation was associated with higher proportions of MPB infestation, but was not associated with having more infestation than expected.

When examining how burn severity varied across the land cover classes (Figure 3-14a), we observed a trend in higher proportions of severe burn in north facing stands than expected, and higher proportions of low, moderate and unburned in south facing stands. The higher severity of north facing stands was more significant within lodgepole stands while the lower severity was more significant for ponderosa stands. Mixed-conifer stands fell in between lodgepole and ponderosa with moderate significance both for north and south facing stands.

If we were to naively combine the two previously discussed sets of trends, we might come to the conclusion that lodgepole pine stands had a higher proportion of MPB infestation and severe burn, therefore there is an association or interaction between the two disturbances. However, this interpretation assumes that the association is between the disturbances and not a separate controlling variable (e.g. lodgepole pine). For example, we did not observe that trend in our four-way mosaic plot of the disturbance interactions (Figure 3-15a). By fitting a log-linear

model of conditional independence and controlling for the land cover classes, we were able to produce residuals that distinguished if the observed frequencies were higher than expected within each land cover class combination.

We observe that the western portion of the High Park Fire primarily consisted of high elevation lodgepole pine stands that experienced an intense MPB outbreak prior to the fire (Figure 3-13a); mortality was first observed in the summer of 2009 (Figure 2-3), approximately a year earlier than the rest of the burn scar. Those stands also experienced the highest proportion of severe vegetation burning from the wildfire (Figure 3-14a), but the MPB infected lodgepole stands did not have a significantly different relative acreage of severe burn than similar uninfected lodgepole stands (Figure 3-15a).

Our analysis did show that forest canopy cover was associated with the proportion of severe burn that uninfected stands experienced. If canopy cover was controlled for, we could either reveal the next largest association or fail to reject the null hypothesis of independence between MPB infestation and burn severity.

5. CONCLUSIONS

In this study we successfully developed a two-tier classification approach for mapping disturbances to forest ecosystem vegetation and utilized it to separately map two stages of MPB infestation and vegetation burn severity for the High Park Fire.

Inspecting the annual differences in the class fraction signature distributions within pixels classified as MPB mortality enabled us to make inferences about the local intensification of the beetle infestation, which we believe alone is enough to recommend the two-tier classification approach. Also, by using the class fraction signatures within the tier-2 classification model we were able to increase our validation accuracies and reduce model over-fitting compared to the tier-1 classification.

Our two-tier approach is applicable to most high or moderate resolution remote sensing platform, but we urge others to consider using the RapidEye satellite constellation because it has an optimal balance of spatial and spectral resolution at a cost that is affordable for landscape level ecological studies. We demonstrated that RapidEye imagery is well suited for high resolution photo interpretation work that allows for digital analysis methods which improve the quality of MPB infestation and burn severity classification maps. A single post-fire image is suitable for the classification of vegetation burn severity as we believe that the current approaches that require a pre-fire image have marginal information gains while unnecessarily restricting the possible remote sensing platforms that may be used.

6. REFERENCES

Bricklemyer, R. S., Lawrence, R. L., Miller, P. R., & Battogtokh, N. (2007). Monitoring and verifying agricultural practices related to soil carbon sequestration with satellite imagery. Agriculture, ecosystems & environment, 118(1), 201-210.

Carroll, A. L., & Safranyik, L. (2003). The bionomics of the mountain pine beetle in lodgepole pine forests: establishing a context. Mountain Pine Beetle symposium: challenges and solutions. Natural Resources Canada, Canadian Forest Service, Pacific Forestry Centre, Information Report BC-X-399, Victoria, BC. 298.

Chavez, P. S. (1988). An improved dark-object subtraction technique for atmospheric scattering correction of multispectral data. Remote sensing of environment, 24(3), 459-479.

Cheng, T., Rivard, B., Sánchez-Azofeifa, G., Feng, J., & Calvo-Polanco, M. (2010). Continuous wavelet analysis for the detection of green attack damage due to mountain pine beetle infestation. Remote Sensing of Environment, 114(4), 899-910.

Cohen, J. (1960). A coefficient of agreement for nominal scales. Educational and Psychological Measurement, 20, 37−46.

Congalton, R. G. (1991). A review of assessing the accuracy of classifications of remotely sensed data. Remote sensing of environment, 37(1), 35-46.

Coops, N. C., Johnson, M., Wulder, M. A., & White, J. C. (2006). Assessment of QuickBird high spatial resolution imagery to detect red attack damage due to mountain pine beetle infestation. Remote Sensing of Environment, 103(1), 67-80.

Friendly, M. (1994). Mosaic displays for multi-way contingency tables. Journal of the American Statistical Association, 89(425), 190-200.

Friendly, M. (1999). Extending mosaic displays: Marginal, conditional, and partial views of categorical data. Journal of Computational and graphical Statistics, 8(3), 373-395.

Fry, J., Coan, M., Homer, C., Meyer, D., & Wickham, J. (2009). Completion of the National Land Cover Database (NLCD) 1992-2001 land cover change retrofit product. Open-file report. US Geological Survey.

Garfin, G., Franco, G., Blanco, H., Comrie, A., Gonzalez, P., Piechota, T., Smyth, R., & Waskom, R. (2014). Chapter 20: Southwest. Climate Change Impacts in the United States: The Third National Climate Assessment. US Global Change Research Program, 462-486.

Gitelson, A. A., & Merzlyak, M. N. (1996). Signature analysis of leaf reflectance spectra: algorithm development for remote sensing of chlorophyll. Journal of plant physiology, 148(3), 494-500.

Hart, S. J., Schoennagel, T., Veblen, T. T., & Chapman, T. B. (2015). Area burned in the western United States is unaffected by recent mountain pine beetle outbreaks. Proceedings of the National Academy of Sciences, 112(14), 4375-4380.

Hartigan, J. A., & Kleiner, B. (1981). Mosaics for contingency tables. Computer Science and Statistics: Proceedings of the 13th Symposium on the Interface. Springer US.

Hicke, J. A., Johnson, M. C., Hayes, J. L., & Preisler, H. K. (2012). Effects of bark beetle-caused tree mortality on wildfire. Forest Ecology and Management, 271, 81-90.

Huang, C., Davis, L., & Townshend, J. (2002). An assessment of support vector machines for land cover classification. International Journal of Remote Sensing, 23(4), 725-749.

Keane, R. E., Ryan, K. C., Veblen, T. T., Allen, C. D., Logan, J. A., & Hawkes, B. (2002). The cascading effects of fire exclusion in Rocky Mountain ecosystems. Rocky Mountain futures: an ecological perspective, 133-152.

Keeley, J. E. (2009). Fire intensity, fire severity and burn severity: a brief review and suggested usage. International Journal of Wildland Fire, 18(1), 116-126.

Krofcheck, D. J., Eitel, J. U., Vierling, L. A., Schulthess, U., Hilton, T. M., Dettweiler-Robinson, E., et al. (2013). Detecting mortality induced structural and functional changes in a piñon-juniper woodland using Landsat and RapidEye time series. Remote Sensing of Environment.

Kurz, W. A., Dymond, C., Stinson, G., Rampley, G., Neilson, E., Carroll, A., et al. (2008). Mountain pine beetle and forest carbon feedback to climate change. Nature, 452(7190), 987-990.

LANDFIRE: LANDFIRE Existing Vegetation Type layer. (2014, September - last update). U.S. Department of Interior, Geological Survey. Available from http://landfire.cr.usgs.gov

Landis, J. R., & Koch, G. G. (1977). The measurement of observer agreement for categorical data. Biometrics, 159-174.

Lefsky, M. A., & Cohen, W. B. (2003). Selection of remotely sensed data. Remote sensing of forest environments, 13-46.

Meddens, A. J., & Hicke, J. A. (2014). Spatial and temporal patterns of Landsat-based detection of tree mortality caused by a mountain pine beetle outbreak in Colorado, USA. Forest Ecology and Management, 322, 78-88.

Meddens, A. J., Hicke, J. A., & Vierling, L. A. (2011). Evaluating the potential of multispectral imagery to map multiple stages of tree mortality. Remote Sensing of Environment, 115(7), 1632-1642.

Miller, J. D., & Thode, A. E. (2007). Quantifying burn severity in a heterogeneous landscape with a relative version of the delta Normalized Burn Ratio (dNBR). Remote Sensing of Environment, 109(1), 66-80.

Paine, R. T., Tegner, M. J., & Johnson, E. A. (1998). Compounded perturbations yield ecological surprises. Ecosystems, 1(6), 535-545.

Quinlan, J. R. (1993). C4. 5: programs for machine learning (Vol. 1). Morgan kaufmann.

Ryan, K. C., & Noste, N. V. (1985). Evaluating prescribed fires. 230.

Safranyik, L. (2003). Mountain pine beetle epidemiology in lodgepole pine. Mountain Pine Beetle symposium: challenges and solutions. Natural Resources Canada, Canadian Forest Service, Pacific Forestry Centre, Information Report BC-X-399, Victoria, BC. 298.

Schoennagel, T., Veblen, T. T., & Romme, W. H. (2004). The interaction of fire, fuels, and climate across Rocky Mountain forests. BioScience, 54(7), 661-676.

Simard, M., Romme, W. H., Griffin, J. M., & Turner, M. G. (2011). Do mountain pine beetle outbreaks change the probability of active crown fire in lodgepole pine forests?. Ecological Monographs, 81(1), 3-24.

Song, C., Woodcock, C. E., Seto, K. C., Lenney, M. P., & Macomber, S. A. (2001). Classification and change detection using Landsat TM data: when and how to correct atmospheric effects?. Remote sensing of Environment, 75(2), 230-244.

Tucker, C. J. (1979). Red and photographic infrared linear combinations for monitoring vegetation. Remote sensing of Environment, 8(2), 127-150.

USDA Forest Service (1950 to present). Annual Aerial Detection Overview Survey. USDA Forest Service, Rocky Mountain Region, Forest Health Management. Available from http://www.fs.usda.gov/detail/r2/forest-grasslandhealth

USDA Forest Service (2013). High Park Fire occurring on the Arapaho & Roosevelt National Forest - 2012 (co4058910540420120609). U.S. Forest Service, Salt Lake City, Utah, USA. Available from http://www.fs.fed.us/postfirevegcondition

USDA Forest Service. (2015). Areas with Tree Mortality from Bark Beetles. Retrieved from http://www.fs.fed.us/foresthealth/technology/pdfs/MpbWestbb_Summary.pdf

USGS EROS (2012). High Park fire near Fort Collins, CO - 2012 (version 2-100% Contained). U.S. Geological Survey, Sioux Falls, South Dakota USA. Available from http://edc.usgs.gov

Walter, J. A., & Platt, R. V. (2013). Multi-temporal analysis reveals that predictors of mountain pine beetle infestation change during outbreak cycles. Forest Ecology and Management, 302, 308-318.

Wulder, M. A., Dymond, C. C., White, J. C., Leckie, D. G., & Carroll, A. L. (2006). Surveying mountain pine beetle damage of forests: A review of remote sensing opportunities. Forest Ecology and Management, 221(1), 27-41.

Wulder, M. A., Ortlepp, S. M., White, J. C., Coops, N. C., & Coggins, S. B. (2009). Monitoring the impacts of mountain pine beetle mitigation. Forest ecology and management, 258(7), 1181-1187.